Chapter 7
Photoreactor Design Aspects and Modeling of Light

Paweł Mazierski, Beata Bajorowicz, Ewelina Grabowska, and Adriana Zaleska-Medynska

Abstract Geometry of the photoreactors depends mainly on the application as well as on the available irradiation source. Additionally, the following factors also need to be considered during the design of photoreactors: (1) type and particle size of the photocatalyst; (2) distribution of the photocatalyst (fixed or suspended); (3) type, content, and distribution of pollutants; (4) mass transfer; (5) fluid dynamics (laminar or turbulent flow); (6) temperature control; (7) reaction mechanism; and (8) reaction kinetics. This chapter deals with the general classification and description of photoreactors used for reaction carried out in the gas and liquid phase. Different types of photoreactors are described in relation to their applications.

Keywords Heterogeneous photocatalysis • Photoreactors • Solar-driven photoreactors • Wastewater treatment • Water disinfection • Air treatment

7.1 Introduction

Since heterogeneous photocatalysis has become an important area of research, it has been applied to various environmental problems including air, water, and wastewater treatment [1], destruction of microorganisms such as bacteria and viruses (disinfection processes) [2, 3], inactivation of cancer cells [4, 5], energy production (hydrogen generation by water splitting, biomass conversion, as well as CO_2 conversion into useful hydrocarbons) [6–12], remediation of oil spills [13], and chemical synthesis [14]. Nevertheless, the accomplishment of the photocatalytic processes at required scale stipulates the use of a photoreactor, a device which allows to contact photons, a photocatalyst, and reactants, as well as to collect the reaction products. In this regard, there are two critical factors and major challenges in the design of photoreactors: (1) how to provide the efficient illumination of the photocatalyst (for a high activity, a large area has to be illuminated) and (2) how to adapt photoreactors for utilization of irradiation provided by

P. Mazierski • B. Bajorowicz • E. Grabowska • A. Zaleska-Medynska (✉)
Department of Environmental Engineering, University of Gdansk, ul. Wita Stwosza 63, 80-308 Gdańsk, Poland
e-mail: adriana.zaleska@ug.edu.pl

J.C. Colmenares, Y.-J. Xu (eds.), *Heterogeneous Photocatalysis*, Green Chemistry and Sustainable Technology, DOI 10.1007/978-3-662-48719-8_7

different sources. Due to the fact that scaling up of photocatalytic reactors is a difficult and complex process, there are some additional factors that also need to be considered, such as the (1) type and particle size of the photocatalyst; (2) distribution of the photocatalyst (fixed or suspended); (3) type, content, and distribution of pollutants; (4) mass transfer; (5) fluid dynamics (laminar or turbulent flow); (6) temperature control; (7) reaction mechanism; and (8) reaction kinetics.

The design of reactor geometry and selection of a photocatalytic reactor depend on the experimental conditions and the specific application. Moreover, the design of large-scale photoreactors must take into account the capacity, ruggedness, reliability, and ease of use. Figure 7.1 illustrates the main types of reactors used for air and wastewater treatment, water splitting, and CO_2, glycerol, and biomass photoconversion. In the liquid phase, the photocatalyst particles are usually suspended in a fluid phase, although other reactor configurations have also been proposed such as packed and fluidized beds with an immobilized photocatalyst. In gas-phase photocatalysis, the most common photoreactors are tubular, annular, and flat-plate types.

Regarding the photocatalyst structural configuration, thin-film powder layer and/or fluidized bed, coated wall-parallel, and honeycomb/foam monolithic reactors are probably the most representative. For photochemical water splitting, batch-type photoreactor is most frequently used configuration in lab-scale investigations. In the case of solar photoreactor systems, there are two of the major design issues: (i) whether to use a suspended or a supported photocatalyst and (ii) whether to use concentrated or non-concentrated sunlight.

The most popular reactors are (1) parabolic trough reactors (PTRs), (2) compound parabolic collecting reactors (CPCRs), and (3) non-concentrating flat-plate reactors which are the double-skin sheet reactor (DSSR).

In addition, it is necessary to pay attention to:

- The type of irradiation: photoreactors can be irradiated using artificial UV light, UV polychromatic lamps, or solar radiation
- The position of the irradiation source: immersed light source, external light source, and distributed light sources such as reflectors or optical fibers

This review deals with the general classification and description of photoreactors used for reaction carried out in the gas and liquid phase. Different types of photoreactors are described in relation to their applications.

7.2 Gas-Phase Photoreactors

Photocatalytic gas-phase reactor should contain two parts: (i) the reactor structure and (ii) source of light. Ideally, the structure of a photocatalytic reactor for air purification should have (i) light source irradiating directly on the photocatalyst surface, (ii) high specific surface area of photocatalyst, and (iii) high mass transfer, low pressure drop, and long residential time. Many types of photocatalytic reactors

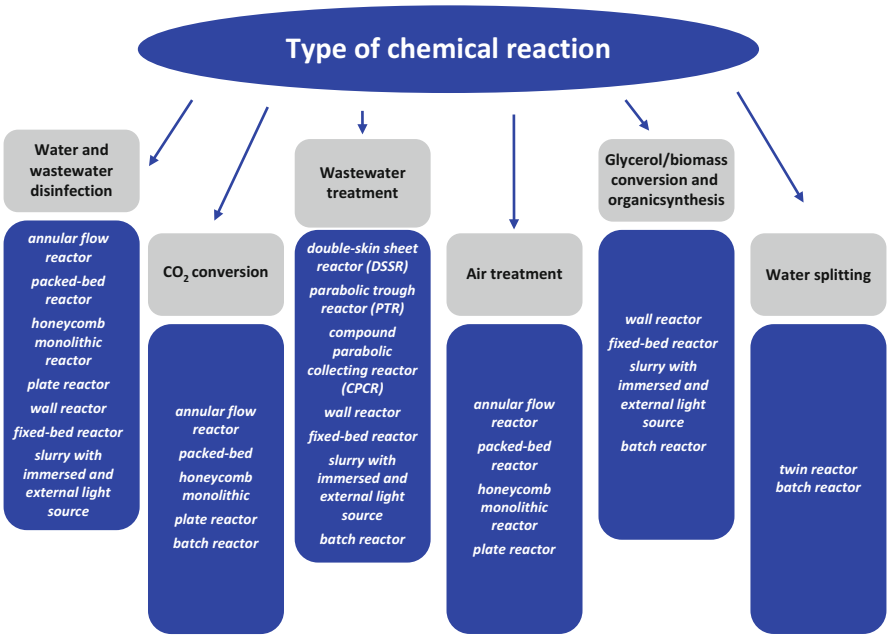

Fig. 7.1 Main types of photoreactors depending on the application

are designed. Annular, plate, slurry, honeycomb monolith, packed bed, and fluidized bed reactors are the most popular, but in the literature, other types are also described: powder layer reactor, with aerosol generator, with optical fibers, and others. However, most of the studies are only based on laboratory scale. Therefore, one of the challenges in the development of photocatalysis for environmental application is the design of efficient reactor that can be used to large-scale commercial application.

7.2.1 Reactors for Photocatalytic Degradation of Volatile Organic Compounds (VOCs)

Generally, the annular reactors are composed of two or more concentric cylindrical tubes mostly made of Pyrex glass. The photocatalyst is coated on the inner wall of the outer cylindrical tubes. The light source is located at the central part of the cylindrical tube. The photocatalyst film coated on the wall of the surface should be thin enough to let all the photocatalyst be irradiated by the light source. Furthermore, source of light can be located outside the reactor, and then thin film of the photocatalyst is coated on the surface of two or more concentric cylindrical tubes. The airflow is provided along the axial direction through the annulus between the lamp and the tube. Figure 7.2a shows one of the types of the annular reactor.

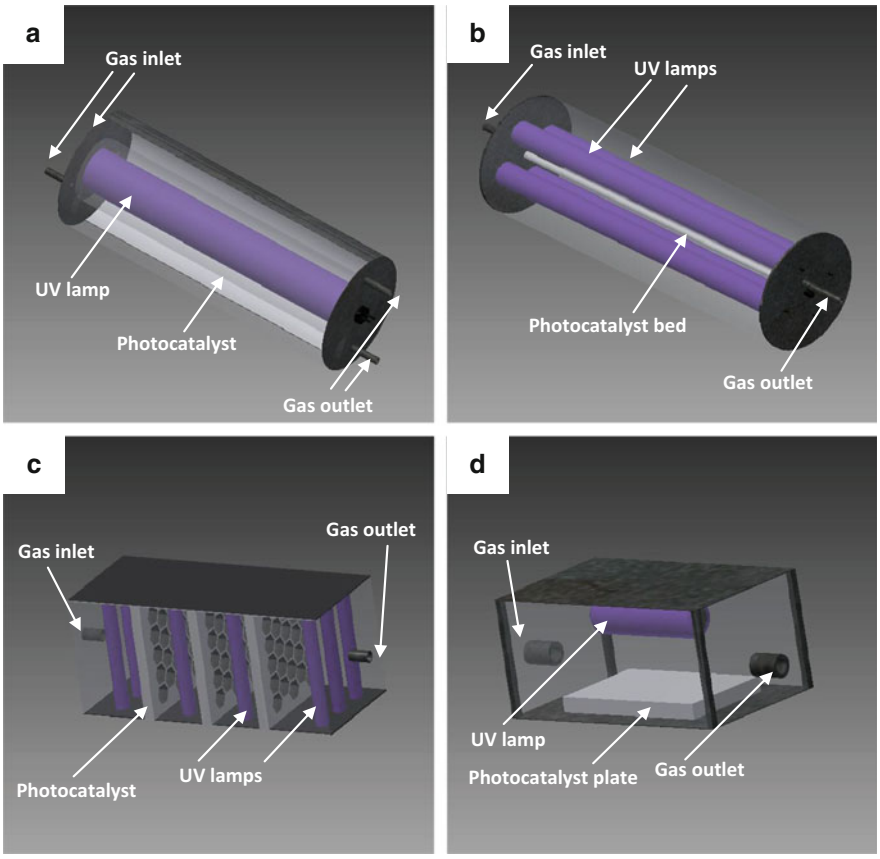

Fig. 7.2 Main types of reactors used for air treatment (**a**) annular, (**b**) packed bed, (**c**) honeycomb monolith, and (**d**) plate

Different types of the annular reactors have been used by several research groups for photocatalytic degradation of volatile organic compounds [15–19].

Tomasic et al. used the annular fixed bed photocatalytic reactor (total volume of the reactor was 0.485 dm^3) to study the degradation of toluene in the gas phase [15]. The P25-TiO_2 thin film was coated on the internal glass surface of the outer tube of the annular reactor. Fluorescent blacklight blue lamp was placed in the central part of the reactor. Tomasic et al. used mathematical models of the photocatalytic reactor (1D model and 2D models based on ideal flow and laminar flow conditions) to understand complex reaction pathways and the reactor's limitation. The obtained models were verified by comparing the computer simulation data with the experimental results. It was found out that photocatalytic reaction carried out in the annular photocatalytic reactor was mainly limited by the interphase mass transfer. Imoberdorf et al. studied the performance of single and multi-annular photocatalytic wall reactor configurations by using a two-dimensional,

reaction–diffusion–convection model and reliable intrinsic reaction kinetics for the photocatalytic degradation of perchloroethylene [16]. The effect of (i) the reactor volume, (ii) the photocatalytic surface area, and (iii) the annulus width on photocatalytic degradation of perchloroethylene in single annular reactor was studied. In the case of multi-annular reactor configurations, the effect on the reactor conversion of (i) the type of flow pattern and (ii) the thickness distribution of TiO_2 films was investigated. It was found that the performance of reactors was strongly influenced by external diffusive resistances; single- and multi-annular photocatalytic reactors present high values of reactor irradiation incidence and photocatalyst irradiation absorption efficiencies. Vincent et al. investigated the photocatalytic oxidation of gaseous 1-propanol by using annular reactor (total volume was 0.0664 dm^3) [17]. The fiberglass support impregnated of P25-TiO_2 was placed between two Pyrex glass tubes. The fiberglass support area exposed to UV irradiation was 0.36 dm^2. 18 W fluorescent tube used as a source of light was located in the center of the reactor. The influence of kinetic parameters such as pollutant concentration, incident light irradiance, contact time, and humidity content has been studied. The authors concluded that the reactor efficiency could be improved in order to reduce the by-product concentrations with other experimental conditions (such as a higher contact time) [17].

The plate reactor, shown in Fig. 7.2d, is the simplest type of photoreactor used for photocatalytic degradation of volatile organic compounds. There are two basic types of plate reactors – with inner and outer source of irradiation. The typical form of this reactor is square or rectangular box, made of different materials (such as stainless steel, plexiglass, or polycarbonate), that is resistant to UV light. Photocatalyst samples used in plate reactors are in the form of powders or flat shape located at the bottom of the reactor. In the case of the plate reactors with inner source of irradiation, a lamp is placed at the upper part of the reactor. In the second one, reactors are equipped with a quartz or borosilicate window, which allows the light passage from lamp into the photocatalyst sample. The advantages of the plate reactor are small pressure drop, the possibility of obtaining large reaction rates, and simplicity. However, the major disadvantage of this type of reactor is the smaller reaction area. Salvado-Estivill et al. used a two-dimensional (2D) analysis of a flat-plate reactor for photocatalytic oxidation of trichloroethylene (TCE) in gas phase under different experimental conditions [20]. The reactor was made of stainless steel (75 mm wide and 600 mm long). A glass plate coated with the photocatalyst (P25-TiO_2) was placed 270 mm from the inlet of the reactor and 170 mm from the outlet. The plate reactor was irradiated by blacklight blue fluorescent lamps. It was found that a two-dimensional model of a flat-plate photocatalytic reactor was shown to approximate closely the experimental results of the photocatalytic oxidation of trichloroethylene. Demeestere et al. used flat-plate reactor to study the photocatalytic degradation kinetics of gaseous trichloroethylene [21]. The reactor was made of stainless steel, with two photocatalyst (P25–TiO_2)-coated glass plates located in the reactor. 18 W blacklight blue lamp used as a source of light was placed over the reactor. The effect of trichloroethylene inlet concentrations (100–500 ppmv), gas residence times (2.5–60.3 s), and relative

humidity (0–62 %) has been investigated. The authors concluded that a trimolecular Langmuir–Hinshelwood model could not fit the experimental results adequately. Therefore, a new kinetic model has been developed, which was based on linear trichloroethylene adsorption–desorption equilibrium and first-order reaction kinetics. Mo et al. studied the by-products during photocatalytic degradation of toluene in a plate reactor [22]. The reactor was made of stainless steel, which two photocatalyst (P25–TiO_2)-coated glass plates located in the reactor. The UVC lamps (Philips Hg lamps) were used to irradiate the photocatalyst plate from the top of the reactor through a quartz glass. It was found that acetaldehyde, methanol, acetone, benzaldehyde, formic acid, ethanol, and acetic acid were the main by-products in the gas-phase toluene degradation.

The packed bed reactors are simple, easy-constructing, and efficient reactor. This type of reactor consists of cylindrical tube made of Pyrex glass, metal, or others. The photocatalyst is located in the central part of the reactor. The source of light can be placed inside or outside reactors. Arabatzis et al. proposed a new packed bed reactor for photocatalytic degradation of volatile organic compounds (VOCs) (see Fig. 7.2b) [23]. The form of this reactor was a cylindrical container made of metal. This container was used to concentrate the emitted light energy from the irradiation source (Sylvania F15w T8/BLBlue lamps). The porous photocatalyst was located on the outer wall of the central glass tube. This reactor has been optimized using theoretical prediction of the conversion factor as a function of the volume, reaction, and molecular feed. Ibhadon et al. presented theoretical study and kinetic modeling of a new packed bed photocatalytic reactor [24]. These results have been confirmed by experimental study on the degradation of benzene, toluene, and xylene. A cylindrical metal container was used to concentrate emitted light energy from four irradiation sources (Sylvania F15WT8/BLBlue lamps). In the central part of cylindrical metal container transparent to UV light, glass tube was located. This tube was filled with the porous P25–TiO_2 photocatalyst. It was found that theoretical and experimental conversion factor was similar and amounted to 96.7 % and 95 %, respectively. This study showed efficient way to design and optimize a packed bed photocatalytic reactor for degradation of VOCs. Fu et al. studied the effect of reaction temperature and water vapor content on the photocatalytic degradation of ethylene using packed bed reactor [25]. The reactor was made of Pyrex tube and was illuminated by four fluorescent UV bulbs. The tube with the bulbs was placed in an insulated cylindrical glass container. It was found that the reaction temperature has a strong influence on the rate of photocatalytic degradation of ethylene under UV light and TiO_2 or Pt/TiO_2 used as photocatalysts. The cause of enhanced photoactivity which was observed at increased reaction temperatures may be due to an enhanced desorption of water from both types of photocatalysts at higher operating temperatures.

Honeycomb monolith reactors are commonly used in automobile exhaust emission control and for NO_x reduction in power-plant flue gases by catalytic reduction, but they also can be used for photocatalytic reactions in the gas phase (see Fig. 7.2c). This type of reactors contains certain number of channels of circular or square cross section. The photocatalyst is coated onto the inner walls of channels

as a thin film. The irradiation source is located in front of the channels. Wang et al. used honeycomb monolith reactor for modeling of formaldehyde photocatalytic degradation using computational fluid dynamics [26]. It was found that distance between the monolith and lamp should be decreased when the number of lamps increases to achieve an optimal configuration. The choice of an optimal number of lamps depends on the flow rate over the monolith. Taranto et al. used an aluminum honeycomb monolith reactor, coated with a thin film of P25–TiO_2 for methane and toluene degradation in the gas phase [27]. As the irradiation source, low-pressure mercury lamps were used. Different types of honeycomb monolith reactors have been used by several research groups for photocatalytic degradation of volatile organic compounds [28, 29].

Fluidized bed reactors are made of transparent container; the treated airstreams pass through container filled with the photocatalyst bed. The light source is located outside of the reactor. The photocatalyst has good contact with the treated airstreams. Fluidized bed reactors can be used to treating fairly high airstreams. Palma et al. used fluidized bed reactor for the intensification of gas-phase photocatalytic oxidative dehydrogenation of cyclohexane [30]. UV irradiation was provided by a two ultraviolet-light-emitting diode (UV-LED) modules located in front of the Pyrex windows. A mathematical modeling was based on Langmuir–Hinshelwood (LH)-type kinetic model. It was found that proposed mathematical model describes the performance of the photocatalytic fluidized bed reactor well for all operating conditions. Hajaghazadeh et al. studied the photocatalytic oxidation of methyl ethyl ketone under UVA light in a fluidized bed reactor [31]. The reactor was made of two parallel quartz windows incorporated in a stainless steel frame. 40 UVA-LEDs were used as an irradiation source and were located in the contact with reactor's quartz windows. Commercial TiO_2 such as P25, PC50, and PC500 was used as a photocatalyst. It was found that the photocatalytic activity depends on the surface area of the photocatalyst.

The batch reactor is the simple type of photoreactors used for VOC degradation. Typically, the batch reactor consists of a chamber made of Pyrex glass. The photocatalyst is located in the lower part of the chamber. The irradiation source is located outside the reactor. Amama et al. used cylindrical batch reactor for photocatalytic degradation of trichloroethylene [32]. The reactor (total volume 0.11 dm^3) was made of Pyrex glass. TiO_2 coated on glass fiber cloth by sol–gel process was used as a photocatalyst and illuminated by eight symmetrically arranged fluorescent blacklight lamps which were located at a fixed distance from the reactor. The authors suggested that photocatalytic degradation of trichloroethylene to carbon dioxide did not occur in the gas phase but mainly at the surface of TiO_2. Additionally, it was found that mineralization yield of trichloroethylene and by-product formation could be affected by pretreatment step of TiO_2, such as preillumination, prehydroxylation, and prechlorination of photocatalyst surface.

Debono et al. used batch reactor for photocatalytic oxidation of decane at ppb levels [33]. This reactor consisted of a Pyrex glass chamber (total volume 120 dm^3) was illuminated by nine PL-L-40 Philips UV lamps. The photocatalyst used for experiments (TiO_2–P25) was placed in the lower part of the reactor chamber. It was found that formaldehyde, acetaldehyde, and propanal were the main by-products formed in the

gas phase during photocatalytic degradation of decane. Moreover, the amounts of these compounds were linearly dependent on the initial decane concentration.

To conclude, many types of photocatalytic reactors for photocatalytic degradation of VOCs have been designed. More examples of reactors are compiled in Table 7.1. The kinetic reaction and mass transfer rate are two of the main

Table 7.1 Reactors used for photocatalytic degradation of volatile organic compounds

Type of the reactor	Material of the reactor	Irradiation source	Photocatalyst	Model of VOCs	Ref.
Annular	Material not claimed	12 W low-pressure Hg lamp	TiO_2 – immobilized in the internal surface of the cylindrical tube	Methyl tert-butyl ether	[34]
				Mixture of benzene, toluene, ethylbenzene, m-, o-, and p-xylene	[35]
				C_5–C_7 alkanes	[36]
	Pyrex reactor made of two coaxial tubes	8 W blacklight lamp	Aeroxide TiO_2P25	Methyl ethyl ketone	[37]
	Two concentric Pyrex tubes	80 W Philips UVA lamp	Glass fiber tissue coated with colloidal silica and TiO_2 nanoparticles.	Isovaleraldehyde	[38]
	Material not claimed	18 W low-pressure Hg lamp	TiO_2 was coated onto the internal glass surface of reactor using dip-coating method	Benzene, toluene, ethylbenzene, and m-xylene	[39]
	Material not claimed	11 W low-pressure Hg lamp	TiO_2, TiO_2/Pt, TiO_2/Fe, TiO_2/Ce- based on P25 and isopropoxide prepared using dip-coating method	Benzene, toluene, ethylbenzene, and m-xylene	[40]
	Open tubular reactors made of Pyrex glass	4 W UVC lamp (Sankyo Denki G4T5)	Commercial P25	Dimethyl sulfide	[41]
	Pyrex glass	6 W UV lamp (Sylvania F6WBLT-6)	Platinum-doped TiO_2, painted on a Pyrex tube	Toluene	[42]
	Pyrex reactor made of two coaxial tubes	24 W solar light-simulating lamp (Philips DeLuxe pro LTJHo)	Commercial P25	Diethyl sulfide	[43]

(continued)

Table 7.1 (continued)

Type of the reactor	Material of the reactor	Irradiation source	Photocatalyst	Model of VOCs	Ref.
Batch	Stainless steel	700 W medium-pressure Hg lamp	Mixed TiO_2 and SiO_2, deposited on the cellulose and synthetic fibers bound	Acetone and 2-butanone	[44]
	Cylindrical Pyrex reactor equipped with a septum	1500 W high-pressure Xe lamp	$Y_xSr_{1-x}TiO_3$	2-Propanol and propene	[45]
	280 cm^3 glass flask	1000 W high-pressure Hg lamp	Multiphase CdS/TiO_2	Ethanol	[46]
	Quartz light window and columnar stainless steel chamber	8 W UVB lamp	Ag and Pt deposited on P25, TiO_2 prepared using sol–gel method	Trichloroethylene, chloroform, dichloromethane, toluene, benzene, carbon tetrachloride	[47]
	120 dm^3 Pyrex chamber	Nine PL-L-40 Phillips UV lamps	TiO_2 powder is sieved on a circular Pyrex plate	Limonene	[48]
	Closed stainless steel reactor with the volume of 105 dm^3	10 W germicidal lamps	TiO_2/Sr_2CeO_4	Benzene	[49]
	Cylindrical bottle with silicon/Teflon Septum	Four blacklight lamps (4 W)	TiO_2 film	2,4,6-Trichloroanisole	[50]
	Cylindrical Pyrex glass reactor	8 symmetrically arranged fluorescent blacklight (160 W)	TiO_2 coated on glass fiber cloth	Trichloroethylene	[51]
	Material not claimed	500 W Xe lamp	TiO_2 nanoparticles	Toluene	[52]
	Reactor made of Pyrex glass, upper part of the reactor was sealed with a Teflon lid	6 W germicidal lamp	TiO_2 coated on the Pyrex glass tube	Trichloroethylene, acetone, methanol, and toluene	[53]
	Closed stainless steel reactor with a volume of 105 dm^3	10 W blacklight lamps	TiO_2 loaded on $Bi_{12}TiO_{20}$	Benzene	[54]

(continued)

Table 7.1 (continued)

Type of the reactor	Material of the reactor	Irradiation source	Photocatalyst	Model of VOCs	Ref.
Optical fiber	Pyrex tube with fused silica optical fibers	500 W UV lamp	TiO_2 coated on the fused silica optical fibers	Benzene	[55]
	Pieces of optical fiber	300 W Xe arc lamp	Quartz fibers coated with TiO_2 layer	Acetone	[56]
Fixed bed	Tubular quartz reactor	Four 4W UV lamps	$BiPO_4$	Benzene	[57]
	Material not claimed	Two 8 W UV lamps	TiO_2 nanoparticles	Hexane, methanol	[58]
	Made of glass tube	Four 6 W UVA lamps	TiO_2 and F-TiO_2 nanoparticles were prepared using sol–gel method	Acetaldehyde and ethanol	[59]
	Rectangle quartz reactor	500 W Xe arc lamp equipped with a UV cutoff filter	Bi_2WO_6-coated carbon microspheres, N-doped TiO_2	Benzene	[60]
Fluidized bed	Made of glass	15 W UVC lamp	TiO_2 coated on the γ-Al_2O_3	Methyl ethyl ketone	[61]
	Concentric double-pipe structure made of Pyrex glass tube	25 W UV lamp	Commercial P25	Cyclohexane	[62]
	Quartz glass tube	10 W and 8 W germicidal white light UV lamps	TiO_2 coated on the silica gel	Trichloroethylene	[63]
Plate	Made of glass	Two germicidal UV lamps	Commercial P25 coated on the glass plate	Vinyl chloride	[64]
	Made of aluminum	Monochromatic germicidal lamps or blacklight lamps	Composite sol–gel TiO_2 and commercial P25 coated on the glass plate	Trichloroethylene and toluene	[65]

parameters having influence for performance of a photocatalytic reactor. Other influencing factors of the reactor efficiency include light of source and intensity, contaminant concentration, humidity, temperature, surface area, and activity of photocatalyst.

7.2.2 Reactors for Photocatalytic Degradation of Inorganic Pollutants

There are various photocatalytic reactors used for oxidation of inorganic pollutants in the gas phase [66–69]. Soylu et al. used flow reactor for photocatalytic oxidation of NO_x [70]. TiO_2–Al_2O_3 photocatalyst was placed on polymethyl methacrylate (PMMA) sample holder inside the reactor. The irradiation was provided by 8 W UVA lamps located outside the reactor. It was found out that TiO_2–Al_2O_3 photocatalyst showed remarkable photocatalytic NO_x oxidation and storage performance in relation to the TiO_2–P25. Dong et al. used flow reactor for photocatalytic NO removal on BiOI surface under the influence of visible light [71]. Photoreactor (4.5 dm^3) was in the form of rectangular box, made of stainless steel, and covered with quartz glass. Testing BiOI film on sample dish was located in the middle of the reactor. A LED lamp was vertically located outside the reactor above the sample dish. Wang et al. used continuous flow reactor for the oxidation of NO from a gaseous phase [72]. Photoreactor was made of Pyrex glass with "Z" type and was irradiated by one 125 W Hg arc lamp located outside the reactor. The volume of the reactor was 340 dm^3. The reactor and source of light were set in a hollow chamber which was coated with tinfoil. Various surfaces platinized TiO_2 were placed in the bottom part of the reactor. Portela et al. used continuous flow flat reactor for photocatalytic oxidation of H_2S [73]. Various photocatalysts were coated on the glass plates. The reactor with a top borosilicate glass window was irradiated by two 8 W UVA lamps. Sheng et al. used continuous flow reactor for photocatalytic oxidation of NO [74]. The woven glass fabric immobilized with photocatalyst was placed into reactor with a "Z" type, made of cylindrical Pyrex glass. 125 W Hg arc lamp used as an irradiation source was located outside the reactor.

Several research groups used fixed bed reactor for photocatalytic oxidation of NO_x, SO_2, and H_2S in the gas phase [75–78]. Liu et al. used fixed bed reactor made of double concentric quartz tubes for oxidation of NO_x and SO_2 [75]. 125 W high-pressure mercury lamp was located in the center of inner tube and was used as an irradiation source. The reactor was placed inside a black box. Cu doped titanium dioxide supported by multi-walled carbon nanotubes was placed in the outer tube. Ou et al. studied photocatalytic oxidation of NO under the influence of visible light using a fixed bed continuous flow reactor [77]. This reactor was made of tubular quartz. The 350 W Xe lamp was vertically placed, parallel with the reactor. The photocatalyst powder (g-C_3N_4/$BiVO_4$) was mixed with silica sand and packed in the reactor. The photocatalytic activity test showed that the maximum conversion of NO was 40 % when the concentration of NO was about 400 ppm under the visible light irradiation Wang et al. used bed reactor for photocatalytic decomposition of H_2S under the influence of visible light [78]. These experiments were carried out in a glass tubular reactor. The 100 W lamp was located outside the reactor. A shutter window was located between the lamp and the reactor to remove UV radiation.

Lafjah et al. studied photocatalytic oxidation of H_2S in the gas phase using single pass annular Pyrex reactor [79]. This reactor was made of two coaxial tubes,

between which the contaminated air was passed through. The irradiation source (8 W blacklight tube) was located inside the internal tube. The photocatalyst powder was placed on the inner surface of the external tube. Tellez et al. used annular reactor for photocatalytic oxidation of H_2S [37, 80]. This type of annular reactor has been described previously.

The plate reactors are often used for photocatalytic oxidation of NO_x in the gas phase [81–86]. These types of reactors were described in the previous subsection. Ao et al. studied photocatalytic oxidation of NO_2 using plate reactor with inner source of irradiation (6 W UV lamp) [81]. The reactor's surface was coated by a Teflon film. TiO_2 powder was coated on the glass fiber filter. Moreover, the plate reactor made of stainless steel with inner source of irradiation was used by Chen et al. for photocatalytic oxidation of NO_x [60, 82]. Yu et al. used plate reactor with outer source of irradiation for removal of NO [83]. This reactor was made of non-adsorbing plastic material. Top of the reactor was covered with a borosilicate plate. The photocatalyst was illuminated by 25 W cool daylight lamps. Other types of the reactors used for photocatalytic oxidation of inorganic pollutants were described elsewhere [87, 88].

7.2.3 Reactors for Photocatalytic Inactivation of Bacteria

Lin et al. used reactor with the commercial TiO_2 filter for photocatalytic inactivation of *Bacillus subtilis* and *Penicillium citrinum* [89]. 8 W fluorescent blacklight lamp was placed above the surface of the filter and glass slide. Photocatalyst-coated filter and irradiation source were located inside the chamber. The spore suspensions of bacteria were dropped directly onto the center part of the TiO_2 filter. TiO_2 filter had a large pore size about 500 μm. Chotigawin et al. used photocatalytic HEPA filter for microorganism disinfection [90]. Two photocatalytic HEPA filters were located into the closed loop chamber side by side. The photocatalyst was irradiated by five 36 W UVA lamps. The photocatalytic filters were made by dip coating a HEPA filter in a P25–TiO_2 slurry. *S. epidermidis*, *B. subtilis*, *A. niger*, *and P. citrinum* were used as the model of microorganism. Vohra et al. investigated the disinfection effectiveness of commercial titanium dioxide coated on the fabric filters for *Bacillus cereus*, *Staphylococcus aureus*, *Escherichia coli*, *Aspergillus niger*, and *MS2 bacteriophage* inactivation [91]. These experiments were carried out in the recirculation duct. The form of this reactor is rectangular in cross section while the lower duct portion is circular.

Keller et al. used the photocatalytic reactor which is a Vigreux-like Pyrex tubular reactor for photocatalytic inactivation of *Escherichia coli* as the model bacteria in airstream [92]. This reactor was made of Pyrex glass. Four 8 W blacklight tubes were located outside the reactor. The photocatalyst was coated on the inside of the tube. This technical solution of the reactor allowed better contact between the solid photocatalyst and flowing bacterial contamination. The reactor consisted of an aerosol generator and a bacterial cultivation medium.

Guo et al. studied photocatalytic inactivation of *Escherichia coli* K12 placed in Petri dish irradiated by two 8 W fluorescent lamps [93]. It was found, that photocatalytic inactivation of microorganism by TiO_2, based on generation of reactive oxygen species (ROS), are followed by action of the generated ROS on the target organism. It was stated that photocatalytic inactivation of bacteria involved oxidative damage of cell walls, membranes, enzymes, and nucleic acids by ROS. Modesto et al. used plate reactor for inactivation of bacteria in the gas phase [94]. *Escherichia coli*, *Bacillus subtilis*, and *Staphylococcus aureus* were used as the model of bacteria. The reactor was made of wooden medium density fiber (MDF) plates of 15 mm thickness. Six glass plates coated with the photocatalyst were located at the lateral walls of the chamber. Four 4 W blacklight lamps were located along the chamber. The suspension of microorganisms in the airstream passed through the reactor. TiO_2, Ag–TiO_2, Pd–TiO_2, and Fe–TiO_2 were used as photocatalysts.

7.2.4 Reactors for Photocatalytic CO_2 Conversion

Photocatalytic CO_2 conversion is carried out in two major system types: (i) two phases and (ii) three phases. Two-phase systems include (i) gas photocatalyst and (ii) liquid photocatalyst. Table 7.2 shows various types of reactors that can be applied for photocatalytic CO_2 conversion in two-phase and three-phase system. It could be concluded that the convective mass transfer rate of CO_2, reaction rate, and surface area of the photocatalyst are the main factors for efficient photocatalytic CO_2 conversion.

Zhao et al. studied photocatalytic reduction of CO_2 in fixed bed reactor [100]. Gas mixture of CO_2, H_2O, and methanol was introduced into a cylindrical reactor made of stainless steel and quartz window. Ag/TiO_2 photocatalyst was coated on the glass fiber filter and placed at the bottom of the reactor. A 150 W solar simulator was located outside the reactor. The same reactor has been used by Liu et al. for photocatalytic reduction of CO_2 in the presence of Cu/TiO_2

Table 7.2 Various types of reactors used for photocatalytic CO_2 conversion in two-phase and three-phase systems

Type of the reactor	Type of CO_2 conversion systems	Ref.
Slurry	Three	[95–97]
Fixed bed	Two	[98, 99]
	Three	[100]
Annular	Two	[101, 102]
Optical fiber	Two	[103–105]
	Three	[106]
Honeycomb monolith	Two	[107]
	Three	[108]

photocatalyst [98]. Shi et al. used fixed bed reactor for photocatalytic conversion of CH_4 and CO_2 to acetone production [109]. The experiments were carried out in a continuous flow quartz fixed bed reactor. A 125 W ultrahigh pressure mercury lamp was located in the center part of the reactor. The photocatalyst bed was placed along the reactor's wall. Cu/CdS–TiO_2/SiO_2 was used as the photocatalyst. Wang et al. used fixed bed reactor for CO_2 reduction with H_2O under simulated solar irradiation [99, 110]. This reactor was made of a stainless steel with the volume of 1.5 dm^3. Photocatalyst powder was placed on the stainless steel omentum located in the center of the reactor. A 300 W Xe arc lamp was put at the top of the quartz window. A moist glass wool was placed between the bottom of the reactor and photocatalyst. The bottom of glass wool support was moisturized of deionized water.

Ola et al. used honeycomb monolith reactor for CO_2 conversion using Pd and Rh–TiO_2 photocatalyst under the influence of ultraviolet irradiation [107]. The optical fibers were uniformly distributed in the monolith and located into a cylindrical reactor made of Pyrex glass. The irradiation was carried out by the high-pressure mercury lamp through the quartz window. The reactor was covered in aluminum foil and located in the gloved box. The experiments were also carried out in the slurry batch annular reactor to comparison quantum efficiency. It was found that the quantum efficiency of the monolith reactor was 23.5 times higher than that of the slurry batch annular reactor due to the high surface area of the monolith and the elimination of uneven light distribution via the optical fibers. Tahir and Amin used microchannel monolith reactor for photocatalytic CO_2 reduction [111, 112]. The reactor was made of a stainless steel cylindrical vessel with a total volume of 0.15 dm^3. The monolith has been coated with photocatalyst and located in the center of the cylindrical reactor, equipped with a quartz window for passing light irradiations from 200 W mercury lamp. The reactor was fitted with heating and cooling jacket to adjust the reactor temperature. The photocatalytic experiment was carried out in a microchannel monolith photoreactor, and its performance was compared with a cell-type photoreactor. It was found that the quantum efficiency achieved in the cell-type reactor was much lower compared to the microchannel monolith reactor due to higher illuminated surface area, higher photon energy consumption, and better utilization of monolith reactor volume.

Nguyen et al. used continuous circular reactor made of Pyrex glass with a quartz window for reduction of CO_2 over ruthenium dye-sensitized TiO_2 metal-doped photocatalysts under concentrated natural sunlight [113]. Photocatalyst was coated on the optical fibers. High-pressure Hg lamp or concentrated natural sunlight was used as the irradiation source. The concentrated natural sunlight was collected by using a solar concentrator and transmitted via an optical cable and focused on the window of the reactor. Wu and Lin used optical fiber reactor for photocatalytic reduction of CO_2 to methanol [104]. Photocatalysts coated on 120 fibers with 16 cm long were located into the reactor. Both sides of the reactor were sealed using O-rings and illuminated from the quartz window of one side by an Hg lamp. The reactor was covered using aluminum foil to avoid the light from the outside during the reaction. Wu et al. studied this same optical fiber reactor for CO_2 reduction

using TiO_2, Cu/TiO_2, and Ag/TiO_2 films coated on 216 fibers as photocatalysts [103].

7.3 Liquid-Phase Photoreactors

There are many types of reactors that can be used in the liquid-phase photocatalytic reactions. The selection usually depends on the experimental conditions and the application. Different water contaminants, ranging from hazardous contaminants of pesticides, herbicides, and detergents to pathogens, viruses, coliforms, etc., can be effectively removed in liquid-phase photoreactors. Table 7.3 summarizes various model compounds and microorganisms commonly used in the photocatalytic reactions. Examples of these various photocatalytic degradation processes and inactivation of the microorganisms will be considered in the following sections.

Liquid-phase heterogeneous photoreactors can be generally divided into three main groups based on their design characteristic such as [114–116]:

1. State of the photocatalyst: reactors with suspended photocatalyst particles (slurry) and reactors with photocatalyst immobilized on the inert surfaces
2. Type of illuminations: artificial light or solar light
3. Position of the irradiation source: external light source, immersed light sources, and distributed light sources (such as reflectors or optical fibers)

While fundamental principles of the photocatalytic processes are relatively well understood, the design and modeling of photocatalytic reactors still require consideration. It is particularly essential in the case of scaled reactors processing large volumes of water and using high levels of irradiation [115, 117].

Table 7.3 Overview of model compounds and microorganisms used for photocatalytic applications

Application	Model compound/microorganism
Photocatalytic degradation of organic pollutants	Methyleneblue [118]; methyl orange [119]; rhodamine B [120], phenol [121]; 4-nitrophenol [122]; trichloroethylene [123]; Congo red [124], chlorophenol [125], tetracycline [126], atrazine [127]
Photocatalytic inactivation of microorganisms	*E. coli* [128]; *Enterococci* [129]; *Bacillus subtilis* [130], *Pseudomonas aeruginosa* [131], *Klebsiella faecal* [132], *Pseudomonas fluorescens*, *Macrococcus caseolyticus* [133], *Salmonella typhimurium* [134], *Bacillus stearothermophilus* [135]

7.3.1 State of the Photocatalyst

7.3.1.1 Slurry Reactors

Slurry reactors are the most common and conventional reactors in photocatalytic technology [136]. In a slurry system, the catalysts are suspended in the liquid phase with the help of mechanical or gas-promoted agitation.

These show the largest photocatalytic activity compared with the immobilized photocatalyst and provide a high total surface area of photocatalyst per unit volume which is one of the most important factors configuring a photoreactor. However, these reactors require an additional downstream separation unit for the recovery of photocatalyst particles [116, 137]. Table 7.4 summarizes the advantages and disadvantages of both slurry and immobilized systems.

The effects of operational parameters on the photocatalytic slurry reactors are systematically investigated to achieve optimum reactor design for more effective photocatalytic water treatment process [115]. Nishio et al. examined the influence of light intensity, initial dye concentration, photocatalyst loading, and initial solution pH on the decolorization rate of Orange II in an external UV light irradiation slurry photoreactor using zinc oxide (ZnO) as a semiconductor photocatalyst. The experiments were performed in a Pyrex glass cylindrical reactor of 0.08 m inside diameter and 0.55 m height. The working volume was 2 dm^3. Around the cylindrical photoreactor were located three 15 W near UV fluorescent lamps (352 nm) and

Table 7.4 The advantages and disadvantages of slurry and immobilized-type reactors [115, 116, 138, 139]

Slurry reactors		Immobilized reactors
Advantages	High total surface area of photocatalyst per unit volume; Simple construction; Potentially lower capital required for a large-scale slurry reactor; Excellent heat transfer performance; Lower catalyst amount than the fixed bed reactor; Well mixed catalyst suspension; Feasibility for large capacity; Low pressure drop; Online removal and addition of catalyst; Limited mass transfer	Continuous operation; Not requiring catalyst recovery; Improved removal organic pollutant from water while using adsorptive materials
Disadvantages	The separation of product and catalyst; Catalyst attrition; Important light scattering and particle; adsorption in the particle suspended; medium	Low surface-area-to-volume ratios; Inherent inefficiencies introduced by light absorption and light scattering in the particle suspension medium; Significant pressure drop; Catalyst fouling or catalyst washout; Mass transfer limitation

externally irradiated the solution. The distance between the lamp and the photoreactor surface was 0.025 m. The photocatalytic reactor as well as lamps was totally covered with an aluminum foil. It was observed that the dye removal efficiency increased as initial pollutant concentration decreased and UV light intensity increased. The highest efficiency was achieved for ZnO concentration being around 1000 mg/dm^3 and pH was around 7.7 [140]. McCullagh presented a novel photoreactor based on a slurry continuous flow reactor configuration for methylene blue (MB) photodegradation in the presence of TiO_2 photocatalyst. This configuration combines the high surface area contact of photocatalyst with pollutant of a slurry reactor and also provides a high illumination of photocatalyst. Moreover, on the inside wall of the reactor vessel, reactor has a unique array of weir-like baffles which continuously remove catalyst from aqueous, enabling the catalyst to be exposed to UV irradiation as the reactor vessel rotates perpendicular to the light source. Experimental results indicated that developed novel reactor configuration exhibited a high UV light penetration characteristic as well as very effective mass transfer rate [141]. In another study, Subramanian et al. reported phenol degradation studies in an annular slurry reactor under various operating and design conditions. The photoreactor had concentric transparent acrylic stationary outer cylinder and inner cylinder rotating at specified revolutions per minute. Authors studied the influence of pollutant concentration (10–50 mg/dm^3), inner cylinder rotation speed (0–50 rpm), catalyst loading (0–8 g/dm^3), annular gap width (7.5, 17.5, and 32.5 mm), as well as mode of illumination: continuous or periodic on the photocatalytic performance. It was clearly demonstrated that the performance of the reactor was improving with the increased content of catalyst, but controlled periodic illumination had no significant influence on reactor efficiency over the regular continuous irradiation. Moreover, rotation of the inner cylinder was necessary only in the case of high gap width configuration at high catalyst loadings [142].

Wang et al. investigated photocatalytic disinfection of gram-negative *Pseudomonas fluorescens* and gram-positive *Macrococcus caseolyticus* spoilage bacteria under various conditions. The reactor system consisted of a magnetic stirrer, a black UV light lamp, and a baker which was exposed to the irradiation from the top. The light intensity was measured using a digital light intensity meter. It was demonstrated that increased photocatalyst contents and UVA light intensity resulted in increased microorganisms killing. Moreover, effectiveness of suspended photocatalyst depended on the initial bacterial population – nano-TiO_2 was more effective against *M. caseolyticus* than *Pseudomonas fluorescens* bacteria [133].

For the photocatalytic reduction of CO_2, in 1979, Inoue et al. introduced a slurry reactor in which catalysts were suspended in water [143]. Until 2000, slurry-type reactors were widely considered for reduction of CO_2 under UV or visible irradiation. On the other hand, Tahir and Amin suggested that this type of reactor is not efficient for enhancing the photocatalytic activity due to the low surface area and complicated separation process required to isolate the miniature catalyst grains [144]. Furthermore, one of the limitations for CO_2 photoreduction in the liquid phase is due to its low solubility in water. Therefore, Rossetti et al. developed an innovative concept of photoreactor, allowing to operate under high pressure (up to

20 bar). The proposed stainless steel reactor was effectively employed to improve CO_2 solubility in a liquid solvent even at high temperature. The suspension was saturated with CO_2 at various temperature and pressure and then irradiated with a 125 W medium-pressure Hg vapor lamp (range of emission: 254–364 nm). The results showed a strong dependence of product distribution on temperature and pressure. An increase of pressure caused increase in CO_2 concentration in the liquid phase and preferred the formation of liquid fuels such as CH_3OH and HCOOH [145].

Priya et al. developed two slurry photocatalytic reactors: batch reactor (BR) (see Fig. 7.3d) and batch-recycle reactor with continuous supply of inert gas (BRRwCG) and compared their performance in the process of hydrogen production. The photoreactors of capacity 300 m leach were made of plexiglass material which was transparent to the solar light. The photocatalytic powders were kept suspended using magnetic stirrer in the BR and gas bubbling and recycling of the suspension in the BRRwCG. The higher generation of hydrogen was observed in the case of BRRwCG due to the recycling of solution and continuous purging of inert gas, enabling the fast desorption of products [146].

7.3.1.2 Immobilized Reactor

Photocatalytic reactors with immobilized photocatalyst are those in which the photocatalyst is fixed to support by physical surface forces or chemical bonds. These reactors extend the benefit of not requiring catalyst recovery and permit the continuous operation [114, 137].

Typical photocatalyst supports are:

- Sand [147]
- Polymer films [148]
- Alumina [149]
- Glass beads [150]
- Zeolite [151]
- Activated carbon [152]
- Silica gel [153, 154]
- Stainless steel [155, 156]
- Carbon fiber [157]

Recently, Li et al. designed novel double-cylindrical-shell (DCS) photoreactor for degradation of rhodamine B (RhB) and methyl orange (MO). The photoreactor was developed by immobilizing TiO_2-coated silica gel beads on the outside surface of interior quartz glass tube of the DCS reactor. In order to optimize designed photocatalytic reactor, the operational parameters such as flow rate, initial concentration, and repetitive operation for the degradation of dye were studied. The developed novel reactor exhibited higher efficiency, lower energy consumption, and better repetitive operation performance for the degradation of RhB and MO as compared with reported slurry and thin-film photoreactors [158]. Behnajady

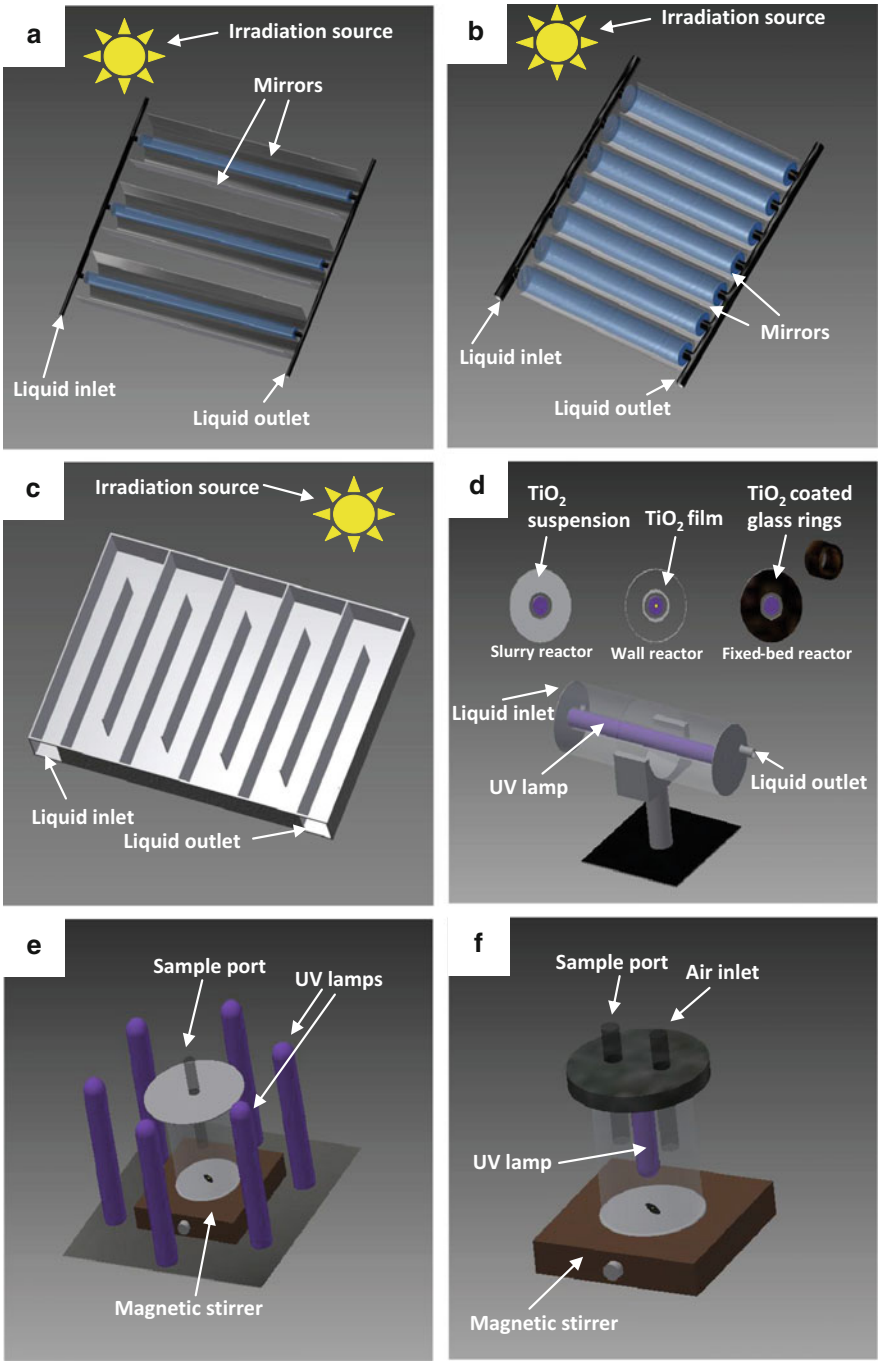

Fig. 7.3 Main types of photoreactors used for water and wastewater treatment (irradiated by sun or UV lamps): (**a**) compound parabolic collector (CPC); (**b**) parabolic trough reactors (PTR); (**c**) double-skin sheet reactor (DSSR); (**d**) slurry, wall, fixed bed reactor; (**e**) batch reactor with outer source of irradiation; and (**f**) batch reactor with inner source of irradiation

et al. described the construction and performance of a continuous flow photoreactor with immobilized TiO_2 on glass plates for photodegradation of C.I. Acid Red 27 (AR27). The photocatalytic reactor consisted of four quartz tubes connected through means of polyethylene tubes from the top to the bottom. Three glass plates loaded with TiO_2–P25 were put into the quartz tubes. Four low-pressure mercury UV lamps were placed in front of the quartz tubes. The results showed that removal efficiency of AR27 increased linearly with increasing the light intensity, but it decreased when the flow rate increased [159].

The reports about photocatalytic disinfection of water commonly use slurry photoreactor, reaching a high efficiency to inactivate microorganisms. However, some efforts have been also concentrated on using immobilized systems, usually exhibiting to be less active and requiring more irradiation time as compared with suspended systems [160, 161]. Grieken et al. developed wall and fixed bed reactors for inactivation of *Escherichia coli*. TiO_2 photocatalyst was immobilized in an annular reactor in two different ways: on the inner reactor wall and on the surface of glass rings used in packed fixed bed reactor. The effect of the increase in the TiO_2 layer thickness has been evaluated, and the results have been compared with those obtained for increasing concentrations of TiO_2 slurries (see Fig. 7.3d). Although immobilized systems were less photoactive than slurry system, they exhibited a higher resistance to the inhibition by organic matter, leading to comparable irradiation time to obtain microorganism concentration below detection limit in wastewater [162].

Hsu et al. immobilized S-doped ZnO nanorods on stainless steel mesh as novel hierarchical photocatalysts for water splitting to hydrogen production. Polymer additive enabled the growth of nanorods on the total surface of wire mesh. The surface texture and photocatalytic hydrogen production performance from salt water under UV light irradiation in a reactor loaded with these photocatalysts were tested. The highest evolution rate was achieved due to increased surface area of the hierarchical immobilized photocatalyst, enhanced light trapping, as well as liquid flow among wire meshes [163].

7.3.2 Type of Irradiation

7.3.2.1 Artificial Light

One of the most challenging parameters in the design of photoreactors is the appropriate illumination of catalyst. Therefore, the important aspects in design consideration for photocatalytic reactors are light wavelength, light intensity, as well as type of irradiation source [115]. There are main types of artificial irradiation sources including: (i) arc lamps, (ii) fluorescent lamps, (iii) incandescent lamps, (iv) lasers, and (v) light-emitting diodes (LEDs). Arc lamps are often named according to the gas contained in the bulb, including neon, argon, xenon, krypton,

Table 7.5 Overview of artificially illuminated liquid-phase photoreactor

Configuration	Catalyst	Light source	Application	Ref.
Labyrinth flow bubble photoreactor	Suspended	Tubular UV lamp (365 nm)	Methyl orange degradation	[165]
Carberry photoreactor	Immobilized	Low-pressure mercury (355 nm)	4-Chlorophenol degradation	[166]
Twin reactor	Suspended	500 W halogen lamp	Hydrogen production	[167]
Batch-recycle reactors	Suspended	Hg-Xe UV lamp	Hydrogen production	[168]
Batch annular reactor	Suspended	9 W Hg lamp	CO_2 photoreduction	[169]
Tubular reactor	Immobilized	Low-pressure mercury lamp	Pollutant degradation	[170]
Fluidized bed reactor	Immobilized	Low-pressure mercury vapor UV lamp	Hydrogen production	[171]

sodium, metal halide, and mercury. Additionally, mercury lamps can be grouped in low, medium, and high-pressure mercury lamp categories [164] (Table 7.5).

Swarnalatha et al. studied photocatalytic oxidation of 2,6-dinitrophenol using different catalysts: TiO_2, TiO_2–P25, CdS, WO_3, and ZnO. The annular-flow photocatalytic reactor used in this research was a cylindrical plastic vessel, in which the mercury lamp is surrounded by a quartz glass tube to belay it from direct contact with an aqueous solution flowing by an annulus between the inner surface of the vessel and the outer surface of the quartz glass tube. It was demonstrated that aqueous TiO_2–P25 suspension exhibited the highest efficiency in photocatalytic degradation at the wavelength of 254 nm using an annular-flow-type reactor equipped with an 8 W low-pressure mercury lamp. Moreover, the effect of irradiation time and pH on the efficiency of degradation was investigated. The pollutant degradation in the presence of P25 was found to incrementally increase with increasing irradiation time at an optimum pH of 8. Complete degradation of the 2,6-dinitrophenol occurred after 3 h of irradiation [172]. In another study, Han et al. investigated photocatalytic degradation of p-chlorobenzoic acid (p-CBA) in aqueous solution using two kinds of low-pressure mercury lamps: UV lamp emitted at 254 nm and the vacuum UV lamp emitted at both 254 nm and 185 nm. The lamp was put in the center of the photocatalytic reactor with quartz tube protection (outer diameter 25 mm). Oxygen or air was used as a bubbling gas which was implemented to the reactor through a porous glass plate with a flow rate of 200 cm^3/min. It could be seen that degradation of p-chlorobenzoic acid was more effective in the presence of vacuum UV lamp than in the case of UV lamp when the same power lamps were used in research [173].

Chen et al. investigated photocatalytic disinfection of *Escherichia coli* K12 using natural sphalerite (NS) as a photocatalyst under various spectra and intensities of visible light emitted by LEDs. The photocatalytic test was performed in the reactor equipped with 16 LED lights and compared with results obtained for two

other visible light sources such as fluorescent tube and xenon lamp. Moreover, photocatalytic disinfection of microorganisms was compared under various single spectra: blue, green, yellow, and red color LEDs. It was shown that the most effective wavelength ranges for photocatalytic inactivation of bacteria are 440–490 and 570–620 nm. Moreover, a positive dependence was observed between the disinfection efficiency and the visible light intensity. The results showed also that NS caused complete inactivation of *E. coli* within 8 h irradiation using white LEDs [174]. In another study, Benabbou et al. examined photocatalytic inactivation of *Escherichia coli* K12. The disinfection experiments were carried out in a Pyrex reactor in which an HPK 125 W lamp emitting in the 200–400 nm range was used as irradiation source. Moreover, various optical filters were used to modify lamp emission spectrum. The light intensity was controlled by grids with various sizes of mesh, which were put on the lamp. The effect of different types of UV light, including UVA, UVB, and UVC was also examined, and modification of the light radiation intensity was discussed. It was found that the addition of photocatalyst at low concentration improved the inactivation of bacteria in the presence of UVA and UVB, but negative effect was noted under UVC. Furthermore, the photocatalytic efficiency increased as a function of light intensity, no matter the experimental conditions [175].

Kočí et al. studied the effect of reactor geometry on the photocatalytic reduction of CO_2 using ZnS nanoparticles deposited on montmorillonite as a catalyst. The photocatalytic experiments were performed in two homemade batch annular reactors with three quartz tubes of various diameters: 3.5, 4.0, and 4.5 cm. The photocatalyst was suspended in NaOH solutions, and after saturation by CO_2, the suspension was illuminated using UV 8 W Hg lamp (254 nm). It was demonstrated that for both reactors, the highest activity of the photocatalytic reduction was obtained in a configuration where the lamp touched the surface of the liquid in the reactor and the configuration of the reactor was not annular. Moreover, it was suggested that one of the most important factors in the slurry reactors is appropriate mixing but its implementation is difficult in apparatus of annular configuration [102].

Hernández-Gordillo et al. investigated photocatalytic activity of CdS photocatalyst for the hydrogen production from either methanol–water or sulfide/sulfite solution in the presence of blue light energy. The photocatalytic tests were performed in a glass homemade photoreactor without any cooling system. The solution was irradiated using blue light emitted by LED lamps of very low power (3 W) which were placed in appropriate positions to allow complete illumination of the suspended catalysts. It was shown that the amount of hydrogen generated linearly increased as a function of the number of LED lamps, achieving to a hydrogen production of 9.54 μmol/h. This study suggested that the hydrogen production depended very strongly on the lamp intensity [176]. In another study, Gomathisankar et al. investigated photocatalytic hydrogen production from aqueous methanol solution using Cu-deposited ZnO photocatalyst. The photocatalytic test was carried out in the Pyrex column vessel reactor. The spout of vessel was hermetic closed with septum and aluminum insulating. The optical filter

($\lambda > 400$ nm) was used for the visible light irradiation. A xenon lamp (500 W) was located on the side of the photoreactor and used as a light source. The light intensity was controlled by a UV radiometer equipped with a sensor of 320–410 nm wavelengths. It was demonstrated that Cu-deposited ZnO had the response to the visible light for the hydrogen production. Furthermore, under the optimal conditions, the photoactivity was about 130 times higher than those showed for bare ZnO photocatalyst [177].

7.3.2.2 Solar Light

The implementation of solar photocatalytic reactors has occurred concurrently with advances in the design of solar thermal collectors. There are specific constraints for the design of solar photocatalytic reactors such as [178, 179]:

- The wastewater must be exposed to ultraviolet solar radiation; therefore, the collector must be made of UV transparent materials.
- Temperature negligible affected the photocatalytic process, so no insulation is required.
- Construction should be economical and efficient with a low pressure drop.

Solar photocatalytic reactors can be divided into concentrating and non-concentrating (one sun) systems depending on received irradiation [180]. - Non-concentrating solar reactors use intensities equal or lesser than natural solar irradiation, while concentrating solar reactors require intensities that surpass irradiations equivalent to one sun [116].

In the concentrating design, solar radiation is collected in a photocatalytic reactor by a reflecting surface, and because of this, for the same light-harvesting area, the reactor volume is smaller than in the case of non-concentrating system [180]. The most promising type of concentrating solar reactor is parabolic trough collector (PTC) which is demonstrated to be efficient for wastewater treatment. PTCs consist of platform that has one or two motors controlled by single- or dual-axis solar tracking system that maintain the collector aperture plane perpendicular to incoming solar radiation (see Fig. 7.3b) [181].

Non-concentrating photoreactors have no moving parts or solar tracking devices (see Fig. 7.3c). This kind of reactor does not concentrate radiation, and because of this, efficiency is not limited by factors connected with reflection, concentration, or solar tracking. In this system, optical efficiency is higher as compared with concentrating reactors. Moreover, non-concentrating system can utilize the diffuse and direct portion of the solar UVA [182]. One-sun collectors are usually cheaper than PTCs because their elements are simpler, and the surface required for their installation is smaller [178].

Compound parabolic collectors (CPCs) belong to the most promising photocatalytic solar reactors which combine the advantages of parabolic trough concentrator and non-concentrating system [178]. CPCs are low-concentration static collectors with reflective surface and can be designed for any given reactor shape (see Fig. 7.3a) [182]. The CPC reflectors are usually made from polished aluminum

because of its high reflectivity in the UV range and high resistance to the environmental conditions. Pipes and valves are manufactured from polyethylene; photoreactor tube is made of borosilicate 25 glass due to high transmission in the UV range of its material. Water flows through the borosilicate tubes to a tank by a centrifugal pump, allowing a turbulent regime inside the photocatalytic reactor [183].

Zayani et al. investigated performances of solar pilot plant for photocatalytic removal of azo dye used as a model pollutant. Experiments were carried out in thin-film fixed bed reactor with an illuminated area of 25 m^2. Effect of important operating parameters including flow rate, catalyst loading, and initial dye concentration on photocatalytic treatment kinetic was examined for optimization which will be necessary in designing large-scale photoreactors. Furthermore, the photodegradation kinetic of total organic carbon (TOC) was discussed in terms of Langmuir–Hinshelwood model [184]. Xu et al. developed novel optical fiber reactor (OFR) in which side-glowing optical fibers (SOFs) were used as light transmission medium as well as photocatalyst supporter. The SOF was made up of quartz core with a silicon cover which can emanate light from side surface more uniformly and transmit light for longer distance. Furthermore, SOF was flexible and can be entwined into any shapes. It was demonstrated that novel reactor can collect solar light efficiency while occupying smaller surface as compared with traditional solar collectors. It was observed that 79 % of 4-chlorophenol decomposed under sunlight irradiation during 8 h [185].

Vidal et al. presented the first pilot-plant study about solar photocatalysis for bacterial inactivation. Researchers constructed a new low-cost compound parabolic concentrator (CPC) prototype containing: solar collector (Pyrex photoreactor tubes, aluminum reflective surface), flowmeter, pump, sensors (pH, O, T, UV radiation), pipes, fittings, and tanks (PVC). This solar photoreactor has an area of 4.5 m^2 and it was tilted at local latitude to maximize the available solar irradiation. It was observed 5-log reduction for *E. coli* and *Enterococcus faecalis* (initial concentration: 10^2–10^4 CFU/cm^3) after 30 min of solar irradiation (solar UV value: 25 W/m^2) [186]. In another study, McLoughlin et al. compared three different solar collectors for the disinfection of water heavily contaminated with *Escherichia coli*. It was demonstrated that three lab-scale solar photoreactors which were constructed using Pyrex tubing and aluminum reflectors of compound parabolic, parabolic, and V-groove profiles all enhance the effect of natural solar irradiation. Among these three collector shapes, compound parabolic reflector promoted the most efficient inactivation of bacteria. Moreover, researchers carried out the tests to assess the improvement to disinfection which could be achieved using TiO_2-coated Pyrex rods fixed within the reactors. However, this solution caused only a slight improvement in performance of the compound parabolic reactor and no enhancement to overall disinfection performance in either the parabolic and V-groove reactors [187]. Alrousan et al. carried out solar photocatalytic disinfection of water using compound parabolic collector and P25 immobilized on borosilicate glass tube. Researchers tested several photoreactor configurations such as (1) borosilicate glass tubes (1.5 m in length) of diameter 50 mm dip coated with TiO_2–P25, (2) uncoated 50 mm borosilicate glass tubes, (3) 32 mm borosilicate glass tube externally dip coated with TiO_2, and (4) uncoated 32 mm borosilicate glass tube.

Each configuration was examined using one tube and one CPC mirror, with an irradiated surface of 0.2 m^2 and a total volume of treated water of 7 dm^3 The most effective configuration was the concentric tube arrangement with CPC [188].

In spite of the still insufficient efficiency of direct photocatalytic water splitting, there are few trials in large-scale application of hydrogen photoreactors in the literature [189]. Jing et al. developed CPC-based solar reactor for photocatalytic hydrogen production that consisted of solar collector, Pyrex photoreactor tubes, reflective surface, and flow meter; fitting, pipes, and tanks; and pump and sensors. The photocatalytic performance was investigated for various design parameters such as tube radius, flow velocity, photocatalyst, as well as sacrificial agent concentrations. In optimal conditions, this photoreactor had higher hydrogen rate per unit volume than in the case of lab-scale reactor which could be caused by the design of tubular reactor properly illuminated by CPC on one side [190]. In another study, Villa et al. tested the simultaneous photocatalytic hydrogen production under direct solar irradiation at pilot-plant scale. The experiments were performed in a compound parabolic collector (CPC) composed of Pyrex glass tube placed on the fixed platform. A centrifugal pump with a flow rate of 20 dm^3/min enabled the recirculation of the aqueous slurry from the tank to the tubes of the photoreactor. The hydrogen was generated from aqueous solutions of formic acid, glycerol, as well as a real wastewater. The highest hydrogen production was obtained with aqueous solution of formic acid after 5 h of irradiation. However, the tests with real wastewater gave moderate amount of hydrogen, suggesting the possible use of such waters for hydrogen production in the future [191].

7.3.3 Position of the Irradiation Source

The arrangement of light source is another important aspect of photocatalytic reactor design. In the case of immersed-type reactor configuration, the lamp is placed inside the unit (see Fig. 7.3e). In external-type reactor, the lamp is located outside the reactor (see Fig. 7.3f). Light has to pass through reactor wall to get the water body. In this kind of reactor, the light intensity and evenness of UV fluence rate (UV-FR) are usually lower than that in the other two types for the same power consumption [192, 193]. Another type is the distributed reactor where light is transported from the source to the photocatalytic reactor using reflectors or light guides [194]. The distributive-type reactor usually is characterized by higher and more uniform irradiation inside the reactor than the external-type reactor.

Effects of different lamp arrangements on photocatalytic reactor performance have not been well studied. Recently, Xu et al. used computational fluid dynamics (CFD) simulation software FLUENT to simulate microorganism particle motion in various UV water disinfection reactors. The influence of lamp arrangements on the UV-FR field and log reduction of different UV water disinfection photoreactors were studied under various flow rates and constant UV dosage. In the experiment, direction, number, and orientation of lamps were diverged. The results showed that

overall effects on the reactor log reduction were complex. Higher water flow rate reduced "barrier" effect in reactors with multiple lamps, lowering log reduction. This study provided new approach for understanding the effect of lamp arrangement on the performance of photodisinfection reactor [193]. Palmisano et al. performed the validation of a two-dimensional model describing the behavior of a batch cylindrical photoreactor, externally irradiated by 1–6 UV fluorescent lamps coupled with a modified Langmuir–Hinshelwood kinetics. Experimental runs were performed at different 4-nitrophenol concentration, Degussa TiO_2–P25 amounts, and under various irradiation configurations. The proposed model allows to determine the behavior of the photoreactor in a wide range of operating conditions: various catalyst and substrate loadings as well as radiations have been applied [195]. Moreover, in the literature, there are a few other reports about models for externally irradiated cylindrical reactors [196, 197].

7.4 Light Modeling

Most of the work in the field of design and modeling of photoreactors was done by Cassano and Alfano [16, 180, 198, 199]. In the case of photoreactor modeling, three main components should be considered: (1) thermal energy balance, (2) multicomponent mass conservation, and (3) photon balance (radiation energy). Balance of photons should be considered independently from the thermal energy balance since the energy useful in photochemical processes is generally negligible. The radiation energy used in the most majority of photochemical processes can be attributed to a range of wavelengths between 200 and 600 nm. *Local volumetric rate of energy absorption* (LVREA), defined as the rate of the radiation-activated step and proportional to the absorbed energy, was preliminarily introduced by Irazoqui et al. [200]. The LVREA depends on the photon distribution in the reaction space. To begin any photochemical reactions, absorption of a photon by a molecule resulted in formation of an excited state is a necessary step. Following absorption of radiation, a few pathways, different from the desired reaction, could be predicted, such as (1) a different, parallel reaction, (2) phosphorescence, (3) fluorescence, (4) deactivation by chemical quenching, etc. In a single-photon absorption process, the rate of radiation-activated step is proportional to the rate of energy absorbed (LVREA). The proportionality constant is the primary reaction quantum yield, defined as:

$$\Phi_{prim,\ v} = \frac{numbermolec_{prim}}{numberphoto_v absorb.}$$

where:

$numbermolec_{prim}$ is the number of molecules following the expected path in the primary process.
$numberphot_v\ absorb.$ is the number of absorbed quanta of radiation.

In most cases, radiation may be arriving at one point inside a photochemical reactor from all directions in space. For a photochemical reaction to take place, this radiation has to be absorbed by an elementary reacting volume described as spectral incident radiation (G_v expressed in W/m^2):

$$G_v = \int_{\Omega} I_v d\Omega$$

where:

I_v is the spectral specific intensity (W/m$^2 \cdot$ sr).
Ω is the unit direction vector (coincides with the axis of an elementary cone of solid angle $d\Omega$).

Thus, to evaluate the LVREA in the case of polychromatic radiation, we have to know the spectral intensity at each point inside the reactor, according to the following equation [198]:

$$e^a = \int_{v1}^{v2} \int_{\theta 1}^{\theta 2} \int_{\phi 1}^{\phi 2} \kappa_v I_v \sin\theta d\phi d\theta dv$$

where:

(θ_1, θ_2) and (Φ_1, Φ_2) are the integration limit that define the space from which radiation arrives at the point of incidence.

7.5 Conclusions

Gas- and liquid-phase photoreactors discussed in this chapter specify the diversity in photocatalytic reactor design along with their potential applications. The following conclusions could be pointed based on the current state of the art in this field:

1. Photoreactors could be generally classified into three main groups based on their design characteristics such as (*i*) *state of the photocatalyst*, reactors with suspended photocatalyst particles (slurry) and reactors with photocatalyst immobilized on the inert surfaces; (*ii*) type of illuminations, artificial light or solar light; and (*iii*) position of the irradiation source, external light source, immersed light sources, and distributed light sources (such as reflectors or optical fibers).
2. Solar-driven large-scale photoreactors are mainly used for water/wastewater treatment and disinfection.
3. Local volumetric rate of energy absorption (LVREA) is defined as the rate of the radiation-activated step in the photochemical reaction and depended on the photon distribution in the reaction space.

Table 7.6 Summary of the principal advantages and disadvantages of gas- and liquid-phase photoreactors

Type of the photoreactor	Advantages	Disadvantages
Liquid-phase photoreactors	Feasibility for large capacity; Very good heat transfer performance; More efficient removal of organic pollutants from water while using adsorptive material	Inherent inefficiencies introduced by light absorption or scattering in the particle suspension medium; Photocatalyst attrition; Possible photocatalyst fouling or washout
Gas phase photoreactors	Relatively low levels of radiation intensity needed to perform reaction; Small amount of photons adsorbed by air and sufficient electron scavengers; Photocatalyst in a form of thin layer – there is no separation of product and photocatalyst; Higher quantum yield of photocatalytic reaction (comparing to liquid phase)	Pollutant adsorption on the walls of the reactor

The advantages and disadvantages of liquid- and gas-phase photoreactors are briefly summarized in Table 7.6.

The industrial application of photocatalytic processes is still limited due to the high cost of UV irradiation light as well as the problem with separation and reusing of photocatalysts after reaction. It could be also assumed that quantum yield in gas-phase reaction is much higher than that one in liquid-phase reaction due to lower light scattering. Therefore, solar-driven or low-powered UV lamp-irradiated (e.g., light-emitting diodes) photoreactors are crucial for broader-scale application of photocatalytic processes. Moreover, the future prospect of photocatalysis cannot rely only on the design of the photoreactors but also on the development of more effective photocatalysts. Photocatalysts used during the processes must achieve greater conversion efficiencies at lower irradiation energies. Finally, visible light-absorbing materials will be the most important component in wide-scale technology.

References

1. Fujishima A, Zhang X (2006) Titanium dioxide photocatalysis: present situation and future approaches. C R Chim 9:750–760
2. Ireland JC, Klostermann P, Rice EW, Clark RM (1993) Inactivation of Escherichia coli by titanium dioxide photocatalytic oxidation. Appl Environ Microbiol 59:1668–1670
3. McCullagh C, Robertson JM, Bahnemann DW, Robertson PK (2007) The application of TiO_2 photocatalysis for disinfection of water contaminated with pathogenic micro-organisms: a review. Res Chem Intermed 33:359–375

4. Cai R, Hashimoto K, Kubota Y, Fujishima A (1992) Increment of photocatalytic killing of cancer cells using TiO_2 with the aid of superoxide dismutase. Chem Lett 21:427–430
5. Cai R, Kubota Y, Shuin T, Sakai H, Hashimoto K, Fujishima A (1992) Induction of cytotoxicity by photoexcited TiO_2 particles. Cancer Res 52:2346–2348
6. Borgarello E, Kiwi J, Pelizzetti E, Visca M, Grätzel M (1981) Photochemical cleavage of water by photocatalysis. Nature 289:158–160
7. Li C, Xi Z, Fang W, Xing M, Zhang J (2015) Enhanced photocatalytic hydrogen evolution activity of $CuInS_2$ loaded TiO_2 under solar light irradiation. J Solid State Chem 226:94–100
8. Wang H, Chen W, Zhang J, Huang C, Mao L (2015) Nickel nanoparticles modified CdS–A potential photocatalyst for hydrogen production through water splitting under visible light irradiation. Int J Hydrog Energy 40:340–345
9. Wang Z, Teramura K, Hosokawa S, Tanaka T (2015) Photocatalytic conversion of CO_2 in water over Ag-modified La_2 Ti_2 O_7. Appl Catal Environ 163:241–247
10. Lee C-W, Kourounioti RA, Wu JC, Murchie E, Maroto-Valer M, Jensen OE, Huang C-W, Ruban A (2014) Photocatalytic conversion of CO_2 to hydrocarbons by light-harvesting complex assisted Rh-doped TiO_2 photocatalyst. J CO_2 Utils 5:33–40
11. Chong R, Li J, Ma Y, Zhang B, Han H, Li C (2014) Selective conversion of aqueous glucose to value-added sugar aldose on TiO_2-based photocatalysts. J Catal 314:101–108
12. Gu Q, Long J, Fan L, Chen L, Zhao L, Lin H, Wang X (2013) Single-site Sn-grafted Ru/TiO_2 photocatalysts for biomass reforming: synergistic effect of dual co-catalysts and molecular mechanism. J Catal 303:141–155
13. Nair M, Luo Z, Heller A (1993) Rates of photocatalytic oxidation of crude oil on salt water on buoyant, cenosphereattached titanium dioxide. Ind Eng Chem Res 32:2318–2323
14. Yoon TP, Ischay MA, Du J (2010) Visible light photocatalysis as a greener approach to photochemical synthesis. Nat Chem 2:527–532
15. Tomašić V, Jović F, Gomzi Z (2008) Photocatalytic oxidation of toluene in the gas phase: modelling an annular photocatalytic reactor. Catal Today 137:350–356
16. Imoberdorf GE, Cassano AE, Irazoqui HA, Alfano OM (2007) Optimal design and modeling of annular photocatalytic wall reactors. Catal Today 129:118–126
17. Vincent G, Marquaire P-M, Zahraa O (2009) Photocatalytic degradation of gaseous 1-propanol using an annular reactor: kinetic modelling and pathways. J Hazard Mater 161:1173–1181
18. Vincent G, Marquaire P-M, Zahraa O (2008) Abatement of volatile organic compounds using an annular photocatalytic reactor: study of gaseous acetone. J Photochem Photobiol A 197:177–189
19. Imoberdorf G, Irazoqui H, Cassano A, Alfano O. Modelling of a multi-annular photoreactor for the degradation of perchloroethylene in gas phase
20. Salvadó-Estivill I, Brucato A, Li Puma G (2007) Two-dimensional modeling of a flat-plate photocatalytic reactor for oxidation of indoor air pollutants. Ind Eng Chem Res 46:7489–7496
21. Demeestere K, De Visscher A, Dewulf J, Van Leeuwen M, Van Langenhove H (2004) A new kinetic model for titanium dioxide mediated heterogeneous photocatalytic degradation of trichloroethylene in gas-phase. Appl Catal Environ 54:261–274
22. Mo J, Zhang Y, Xu Q, Zhu Y, Lamson JJ, Zhao R (2009) Determination and risk assessment of by-products resulting from photocatalytic oxidation of toluene. Appl Catal Environ 89:570–576
23. Arabatzis I, Spyrellis N, Loizos Z, Falaras P (2005) Design and theoretical study of a packed bed photoreactor. J Mater Process Technol 161:224–228
24. Ibhadon A, Arabatzis I, Falaras P, Tsoukleris D (2007) The design and photoreaction kinetic modeling of a gasphase titania foam packed bed reactor. Chem Eng J 133:317–323
25. Fu X, Clark LA, Zeltner WA, Anderson MA (1996) Effects of reaction temperature and water vapor content on the heterogeneous photocatalytic oxidation of ethylene. J Photochem Photobiol A 97:181–186

26. Wang X, Tan X, Yu T (2014) Modeling of formaldehyde photocatalytic degradation in a honeycomb monolith reactor using computational fluid dynamics. Ind Eng Chem Res 53:18402–18410
27. Taranto J, Frochot D, Pichat P (2009) Photocatalytic air purification: comparative efficacy and pressure drop of a TiO_2-coated thin mesh and a honeycomb monolith at high air velocities using a 0.4 m 3 close-loop reactor. Sep Purif Technol 67:187–193
28. Wei D, Vanderspurt T, Hay S, Schmidt W, Obee T, Wei D, H. VT, O HS, R SW, N OT (2005) Bifunctional layered photocatalyst/thermocatalyst for improving indoor air quality
29. Wei D, Obee TN, Hay SO, Vanderspurt TH, Schmidt WR, Sangiovanni JJ (2007) C. Corporation, oxidation impurities in air; applying ultraviolet radiation to oxidation catalyst; activation
30. Palma V, Sannino D, Vaiano V, Ciambelli P (2010) Fluidized-bed reactor for the intensification of gas-phase photocatalytic oxidative dehydrogenation of cyclohexane. Ind Eng Chem Res 49:10279–10286
31. Hajaghazadeh M, Vaiano V, Sannino D, Kakooei H, Sotudeh-Gharebagh R, Ciambelli P (2014) Heterogeneous photocatalytic oxidation of methyl ethyl ketone under UV-A light in an LED-fluidized bed reactor. Catal Today 230:79–84
32. Amama PB, Itoh K, Murabayashi M (2002) Gas-phase photocatalytic degradation of trichloroethylene on pretreated TiO_2. Appl Catal Environ 37:321–330
33. Debono O, Thévenet F, Gravejat P, Hequet V, Raillard C, Le Coq L, Locoge N (2013) Gas phase photocatalyticoxidation of decane at ppb levels: removal kinetics, reaction intermediates and carbon mass balance. J Photochem Photobiol A 258:17–29
34. Boulamanti AK, Philippopoulos CJ (2008) Photocatalytic degradation of methyl tert-butyl ether in the gas-phase: a kinetic study. J Hazard Mater 160:83–87
35. Boulamanti AK, Korologos CA, Philippopoulos CJ (2008) The rate of photocatalytic oxidation of aromatic volatile organic compounds in the gas-phase. Atmos Environ 42:7844–7850
36. Boulamanti AK, Philippopoulos CJ (2009) Photocatalytic degradation of C_5–C_7 alkanes in the gas–phase. Atmos Environ 43:3168–3174
37. Alonso-Tellez A, Masson R, Robert D, Keller N, Keller V (2012) Comparison of Hombikat UV100 and P_{25} TiO_2 performance in gas-phase photocatalytic oxidation reactions. J Photochem Photobiol A 250:58–65
38. Assadi AA, Palau J, Bouzaza A, Wolbert D (2013) Modeling of a continuous photocatalytic reactor for isovaleraldehyde oxidation: effect of different operating parameters and chemical degradation pathway. Chem Eng Res Des 91:1307–1316
39. Korologos CA, Philippopoulos CJ, Poulopoulos SG (2011) The effect of water presence on the photocatalytic oxidation of benzene, toluene, ethylbenzene and m-xylene in the gas-phase. Atmos Environ 45:7089–7095
40. Korologos CA, Nikolaki MD, Zerva CN, Philippopoulos CJ, Poulopoulos SG (2012) Photocatalytic oxidation of benzene, toluene, ethylbenzene and m-xylene in the gas-phase over TiO_2-based catalysts. J Photochem Photobiol A 244:24–31
41. Lee DM, Yun HJ, Yu S, Yun SJ, Lee SY, Kang SH, Yi J (2012) Design of an efficient photocatalytic reactor for the decomposition of gaseous organic contaminants in air. Chem Eng J 187:203–209
42. Colón G, Maicu M, Hidalgo M, Navío J, Kubacka A, Fernández-García M (2010) Gas phase photocatalytic oxidation of toluene using highly active Pt doped TiO_2. J Mol Catal A 320:14–18
43. Grandcolas M, Cottineau T, Louvet A, Keller N, Keller V (2013) Solar light-activated photocatalytic degradation of gas phase diethylsulfide on WO_3-modified TiO_2 nanotubes. Appl Catal Environ 138:128–140
44. Raillard C, Hequet V, Le Cloirec P, Legrand J (2004) Kinetic study of ketones photocatalytic oxidation in gas phase using TiO_2-containing paper: effect of water vapor. J Photochem Photobiol A 163:425–431

45. García-López E, Marcì G, Megna B, Parisi F, Armelao L, Trovarelli A, Boaro M, Palmisano L (2015) $SrTiO_3$- based perovskites: preparation, characterization and photocatalytic activity in gas–solid regime under simulated solar irradiation. J Catal 321:13–22
46. Kozlova EA, Kozhevnikova NS, Cherepanova SV, Lyubina TP, Gerasimov EY, Kaichev VV, Vorontsov AV, Tsybulya SV, Rempel AA, Parmon VN (2012) Photocatalytic oxidation of ethanol vapors under visible light on CdS–TiO_2 nanocatalyst. J Photochem Photobiol A 250:103–109
47. Zuo G-M, Cheng Z-X, Chen H, Li G-W, Miao T (2006) Study on photocatalytic degradation of several volatile organic compounds. J Hazard Mater 128:158–163
48. Ourrad H, Thevenet F, Gaudion V, Riffault V (2015) Limonene photocatalytic oxidation at ppb levels: assessment of gas phase reaction intermediates and secondary organic aerosol heterogeneous formation. Appl Catal Environ 168:183–194
49. Zhong J, Wang J, Tao L, Gong M, Zhimin L, Chen Y (2007) Photocatalytic degradation of gaseous benzene over TiO_2/Sr_2 CeO_4: kinetic model and degradation mechanisms. J Hazard Mater 139:323–331
50. Vlachos P, Stathatos E, Lyberatos G, Lianos P (2008) Gas-phase photocatalytic degradation of 2, 4, 6- trichloroanisole in the presence of a nanocrystalline Titania film. Applications to the treatment of cork stoppers. Catal Commun 9:1987–1990
51. Amama PB, Itoh K, Murabayashi M (2004) Photocatalytic degradation of trichloroethylene in dry and humid atmospheres: role of gas-phase reactions. J Mol Catal A 217:109–115
52. Inaba R, Fukahori T, Hamamoto M, Ohno T (2006) Synthesis of nanosized TiO_2 particles in reverse micellesystems and their photocatalytic activity for degradation of toluene in gas phase. J Mol Catal A 260:247–254
53. Kim SB, Hwang HT, Hong SC (2002) Photocatalytic degradation of volatile organic compounds at the gas–solid interface of a TiO_2 photocatalyst. Chemosphere 48:437–444
54. Lin T, Pi Z, Gong MC, Zhong JB, Wang JL, Chen YQ (2007) Gas-phase photocatalytic oxidation of benzene over titanium dioxide loaded on Bi_{12} TiO_20. Chin Chem Lett 18:241–243
55. Wang W, Ku Y, Ma C, Jeng F (2005) Modeling of the photocatalytic decomposition of gaseous benzene in a TiO_2 coated optical fiber photoreactor. J Appl Electrochem 35:709–714
56. Choi W, Ko JY, Park H, Chung JS (2001) Investigation on TiO_2-coated optical fibers for gas-phase photocatalytic oxidation of acetone. Appl Catal Environ 31:209–220
57. Long B, Huang J, Wang X (2012) Photocatalytic degradation of benzene in gas phase by nanostructured $BiPO_4$ catalysts. Prog Nat Sci 22:644–653
58. Wu C, Yue Y, Deng X, Hua W, Gao Z (2004) Investigation on the synergetic effect between anatase and rutile nanoparticles in gas-phase photocatalytic oxidations. Catal Today 93:863–869
59. Jiang Y, Amal R (2013) Selective synthesis of TiO_2-based nanoparticles with highly active surface sites for gasphase photocatalytic oxidation. Appl Catal Environ 138:260–267
60. Chen Y, Cao X, Kuang J, Chen Z, Chen J, Lin B (2010) The gas-phase photocatalytic mineralization of benzene over visible-light-driven Bi_2WO_6@C microspheres. Catal Commun 12:247–250
61. Dashliborun AM, Sotudeh-Gharebagh R, Hajaghazadeh M, Kakooei H, Afshar S (2013) Modeling of the photocatalytic degradation of methyl ethyl ketone in a fluidized bed reactor of nano-TiO_2/γ-Al_2 O_3 particles. Chem Eng J 226:59–67
62. Geng Q, Wang Q, Zhang Y, Wang L, Wang H (2013) Photocatalytic degradation intrinsic kinetics of gaseous cyclohexane in a fluidized bed photocatalytic reactor. Res Chem Intermed 39:1711–1726
63. Lim TH, Kim SD (2004) Photo-degradation characteristics of TCE (trichloroethylene) in an annulus fluidized bed photoreactor. Korean J Chem Eng 21:905–909
64. Mohseni M, Taghipour F (2004) Experimental and CFD analysis of photocatalytic gas phase vinyl chloride (VC) oxidation. Chem Eng Sci 59:1601–1609

65. Keshmiri M, Troczynski T, Mohseni M (2006) Oxidation of gas phase trichloroethylene and toluene using composite sol–gel TiO_2 photocatalytic coatings. J Hazard Mater 128:130–137
66. Ou M, Dong F, Zhang W, Wu Z (2014) Efficient visible light photocatalytic oxidation of NO in air with band-gap tailored $(BiO)_2$ CO_3–BiOI solid solutions. Chem Eng J 255:650–658
67. Polat M, Soylu AM, Erdogan DA, Erguven H, Vovk EI, Ozensoy E (2015) Influence of the sol–gel preparation method on the photocatalytic NO oxidation performance of TiO_2/Al_2O_3 binary oxides. Catal Today 241:25–32
68. Sugrañez R, Álvarez J, Cruz-Yusta M, Mármol I, Morales J, Vila J, Sánchez L (2013) Enhanced photocatalytic degradation of NO_x gases by regulating the microstructure of mortar cement modified with titanium dioxide. Build Environ 69:55–63
69. Menéndez-Flores VM, Bahnemann DW, Ohno T (2011) Visible light photocatalytic activities of S-doped TiO_2-Fe^{3+} in aqueous and gas phase. Appl Catal Environ 103:99–108
70. Soylu AM, Polat M, Erdogan DA, Say Z, Yıldırım C, Birer Ö, Ozensoy E (2014) TiO_2–Al_2O_3 binary mixed oxide surfaces for photocatalytic NO_x abatement. Appl Surf Sci 318:142–149
71. Dong G, Ho W, Zhang L (2015) Photocatalytic NO removal on BiOI surface: the change from nonselective oxidation to selective oxidation. Appl Catal Environ 168:490–496
72. Wang H, Wu Z, Liu Y, Wang Y (2009) Influences of various Pt dopants over surface platinized TiO_2 on the photocatalytic oxidation of nitric oxide. Chemosphere 74:773–778
73. Portela R, Suárez S, Rasmussen S, Arconada N, Castro Y, Durán A, Ávila P, Coronado J, Sánchez B (2010) Photocatalytic-based strategies for H_2S elimination. Catal Today 151:64–70
74. Sheng Z, Wu Z, Liu Y, Wang H (2008) Gas-phase photocatalytic oxidation of NO over palladium modified TiO_2 catalysts. Catal Commun 9:1941–1944
75. Liu H, Yu X, Yang H (2014) The integrated photocatalytic removal of SO_2 and NO using Cu doped titaniumdioxide supported by multi-walled carbon nanotubes. Chem Eng J 243:465–472
76. Signoretto M, Ghedini E, Trevisan V, Bianchi C, Ongaro M, Cruciani G (2010) TiO_2–MCM-41 for the photocatalytic abatement of NO_x in gas phase. Appl Catal Environ 95:130–136
77. Ou M, Zhong Q, Zhang S, Yu L (2015) Ultrasound assisted synthesis of heterogeneous $gC_3N_4/BiVO_4$ composites and their visible-light-induced photocatalytic oxidation of NO in gas phase. J Alloys Compd 626:401–409
78. Wang Z, Ci X, Dai H, Yin L, Shi H (2012) One-step synthesis of highly active Ti-containing Cr-modified MCM-48 mesoporous material and the photocatalytic performance for decomposition of H_2S under visible light. Appl Surf Sci 258:8258–8263
79. Lafjah M, Mayoufi A, Schaal E, Djafri F, Bengueddach A, Keller N, Keller V (2014) TiO_2 nanorods for gas phase photocatalytic applications. Catal Today 235:193–200
80. Alonso-Tellez A, Robert D, Keller N, Keller V (2012) A parametric study of the UV-A photocatalytic oxidation of H_2S over TiO_2. Appl Catal Environ 115:209–218
81. Ao C, Lee S, Mak C, Chan L (2003) Photodegradation of volatile organic compounds (VOCs) and NO for indoor air purification using TiO_2: promotion versus inhibition effect of NO. Appl Catal Environ 42:119–129
82. Chen M, Liu Y (2010) NO_x removal from vehicle emissions by functionality surface of asphalt road. J Hazard Mater 174:375–379
83. Yu Q, Brouwers H (2009) Indoor air purification using heterogeneous photocatalytic oxidation. Part I: experimental study. Appl Catal B 92:454–461
84. Nguyen NH, Bai H (2014) Photocatalytic removal of NO and NO_2 using titania nanotubes synthesized by hydrothermal method. J Environ Sci 26:1180–1187
85. Hüsken G, Hunger M, Brouwers H (2009) Experimental study of photocatalytic concrete products for air purification. Build Environ 44:2463–2474
86. Toma F-L, Bertrand G, Chwa SO, Meunier C, Klein D, Coddet C (2006) Comparative study on the photocatalytic decomposition of nitrogen oxides using TiO_2 coatings prepared by conventional plasma spraying and suspension plasma spraying. Surf Coat Technol 200:5855–5862

87. Krishnan P, Zhang M-H, Cheng Y, Riang DT, Liya EY (2013) Photocatalytic degradation of SO_2 using TiO_2- containing silicate as a building coating material. Construct Build Mater 43:197–202
88. Martinez T, Bertron A, Ringot E, Escadeillas G (2011) Degradation of NO using photocatalytic coatings applied to different substrates. Build Environ 46:1808–1816
89. Lin C-Y, Li C-S (2003) Inactivation of microorganisms on the photocatalytic surfaces in air. Aerosol Sci Technol 37:939–946
90. Chotigawin R, Sribenjalux P, Supothina S, Johns J, Charerntanyarak L, Chuaybamroong P (2010) Airborne microorganism disinfection by photocatalytic HEPA filter. Environment Asia 3:1–7
91. Vohra A, Goswami D, Deshpande D, Block S (2006) Enhanced photocatalytic disinfection of indoor air. Appl Catal Environ 64:57–65
92. Keller V, Keller N, Ledoux MJ, Lett M-C (2005) Biological agent inactivation in a flowing air stream by photocatalysis. Chem Commun 23:2918–2920
93. Guo M-Z, Ling T-C, Poon C-S (2012) TiO_2-based self-compacting glass mortar: comparison of photocatalytic nitrogen oxide removal and bacteria inactivation. Build Environ 53:1–6
94. Modesto O, Hammer P, Nogueira RFP (2013) Gas phase photocatalytic bacteria inactivation using metal modified TiO_2 catalysts. J Photochem Photobiol A 253:38–44
95. Slamet HWN, Purnama E, Riyani K, Gunlazuardi J (2009) Effect of copper species in a photocatalytic synthesis of methanol from carbon dioxide over copper-doped titania catalysts. World Appl Sci J 6:112–122
96. Wang Q, Wu W, Chen J, Chu G, Ma K, Zou H (2012) Novel synthesis of ZnPc/TiO_2 composite particles and carbon dioxide photo-catalytic reduction efficiency study under simulated solar radiation conditions. Colloids Surf A Physicochem Eng Asp 409:118–125
97. Lee W-H, Liao C-H, Tsai M-F, Huang C-W, Wu JC (2013) A novel twin reactor for CO_2 photoreduction to mimic artificial photosynthesis. Appl Catal Environ 132:445–451
98. Liu L, Gao F, Zhao H, Li Y (2013) Tailoring Cu valence and oxygen vacancy in Cu/TiO_2 catalysts for enhanced CO_2 photoreduction efficiency. Appl Catal Environ 134:349–358
99. Wang Y, Li B, Zhang C, Cui L, Kang S, Li X, Zhou L (2013) Ordered mesoporous CeO_2-TiO_2 composites: highly efficient photocatalysts for the reduction of CO_2 with H_2O under simulated solar irradiation. Appl Catal Environ 130:277–284
100. Zhao C, Krall A, Zhao H, Zhang Q, Li Y (2012) Ultrasonic spray pyrolysis synthesis of Ag/TiO_2 nanocomposite photocatalysts for simultaneous H_2 production and CO_2 reduction. Int J Hydrog Energy 37:9967–9976
101. Kočí K, Matějka V, Kovář P, Lacný Z, Obalová L (2011) Comparison of the pure TiO_2 and kaolinite/TiO_2 composite as catalyst for CO_2 photocatalytic reduction. Catal Today 161:105–109
102. Kočí K, Reli M, Kozák O, Lacný Z, Plachá D, Praus P, Obalová L (2011) Influence of reactor geometry on the yield of CO_2 photocatalytic reduction. Catal Today 176:212–214
103. Wu JC, Wu T-H, Chu T, Huang H, Tsai D (2008) Application of optical-fiber photoreactor for CO_2 photocatalytic reduction. Top Catal 47:131–136
104. Wu J, Lin H-M (2005) Photo reduction of CO_2 to methanol via TiO_2 photocatalyst. Int J Photoenergy 7:115–119
105. Zhao Z-H, Fan J-M, Wang Z-Z (2007) Photo-catalytic CO_2 reduction using sol–gel derived titania-supported zinc-phthalocyanine. J Clean Prod 15:1894–1897
106. Guan G, Kida T, Harada T, Isayama M, Yoshida A (2003) Photoreduction of carbon dioxide with water over $K_2Ti_6O_{13}$ photocatalyst combined with Cu/ZnO catalyst under concentrated sunlight. Appl Catal Gen 249:11–18
107. Ola O, Maroto-Valer M, Liu D, Mackintosh S, Lee C-W, Wu JC (2012) Performance comparison of CO_2 conversion in slurry and monolith photoreactors using Pd and Rh-TiO_2 catalyst under ultraviolet irradiation. Appl Catal Environ 126:172–179

108. Liou P-Y, Chen S-C, Wu JC, Liu D, Mackintosh S, Maroto-Valer M, Linforth R (2011) Photocatalytic CO_2 reduction using an internally illuminated monolith photoreactor. Energy Environ Sci 4:1487–1494
109. Shi D, Feng Y, Zhong S (2004) Photocatalytic conversion of CH_4 and CO_2 to oxygenated compounds over Cu/CdS–TiO_2/SiO_2 catalyst. Catal Today 98:505–509
110. Wang Y, Wang F, Chen Y, Zhang D, Li B, Kang S, Li X, Cui L (2014) Enhanced photocatalytic performance of ordered mesoporous Fe-doped CeO_2 catalysts for the reduction of CO_2 with H_2O under simulated solar irradiation. Appl Catal Environ 147:602–609
111. Tahir M, Amin NS (2013) Photocatalytic CO_2 reduction and kinetic study over In/TiO_2 nanoparticles supported microchannel monolith photoreactor. Appl Catal Gen 467:483–496
112. Tahir M, Amin NS (2013) Photocatalytic CO_2 reduction with H_2O vapors using montmorillonite/TiO_2 supported microchannel monolith photoreactor. Chem Eng J 230:314–327
113. Nguyen T-V, Wu JC, Chiou C-H (2008) Photoreduction of CO_2 over ruthenium dye-sensitized TiO_2-based catalysts under concentrated natural sunlight. Catal Commun 9:2073–2076
114. McCullagh C, Skillen N, Adams M, Robertson PK (2011) Photocatalytic reactors for environmental remediation: a review. J Chem Technol Biotechnol 86:1002–1017
115. Chong MN, Jin B, Chow CWK, Saint C (2010) Recent developments in photocatalytic water treatment technology: a review. Water Res 44:2997–3027
116. De Lasa H, Serrano B, Salaices M (2005) Photocatalytic reaction engineering. Springer, New york
117. Ibhadon A, Fitzpatrick P (2013) Heterogeneous photocatalysis: recent advances and applications. Catalysts 3:189–218
118. Wetchakun N, Chainet S, Phanichphant S, Wetchakun K (2015) Efficient photocatalytic degradation of methylene blue over $BiVO_4$/TiO_2 nanocomposites. Ceram Int 41:5999–6004
119. Zhang L, Zhang J, Zhang W, Liu J, Zhong H, Zhao Y (2015) Photocatalytic activity of attapulgite–BiOCl–TiO_2 toward degradation of methyl orange under UV and visible light irradiation. Mater Res Bull 66:109–114
120. Xu W, Fang J, Chen Y, Lu S, Zhou G, Zhu X, Fang Z (2015) Novel heterostructured Bi_2S_3/$Bi_2Sn_2O_7$ with highlyvisible light photocatalytic activity for the removal of rhodamine B. Mater Chem Phys 154:30–37
121. Kunduz S, Soylu GSP (2015) Highly active $BiVO_4$ nanoparticles: the enhanced photocatalytic properties under natural sunlight for removal of phenol from wastewater. Sep Purif Technol 141:221–228
122. Chen J, Zhang H, Liu P, Li Y, Liu X, Li G, Wong PK, An T, Zhao H (2015) Cross-linked $ZnIn_2S_4$/rGO composite photocatalyst for sunlight-driven photocatalytic degradation of 4-nitrophenol. Appl Catal Environ 168–169:266–273
123. Lee D-S, Park S-J (2015) Water-mediated modulation of TiO_2 decorated with graphene for photocatalytic degradation of trichloroethylene. Curr Appl Phys 15:144–148
124. Habibi MH, Rahmati MH (2015) The effect of operational parameters on the photocatalytic degradation of Congo red organic dye using ZnO–CdS core–shell nano-structure coated on glass by Doctor Blade method. Spectrochim Acta A Mol Biomol Spectrosc 137:160–164
125. Yamazaki S, Yamate T, Adachi K (2013) Photocatalytic activity of aqueous WO_3 sol for the degradation of Orange II and 4-chlorophenol. Appl Catal Gen 454:30–36
126. Yan X, Wang X, Gu W, Wu M, Yan Y, Hu B, Che G, Han D, Yang J, Fan W, Shi W (2015) Single-crystalline $AgIn(MoO_4)_2$ nanosheets grafted Ag/AgBr composites with enhanced plasmonic photocatalytic activity for degradation of tetracycline under visible light. Appl Catal Environ 164:297–304
127. Zhang Y, Han C, Nadagouda MN, Dionysiou DD (2015) The fabrication of innovative single crystal N, Fcodoped titanium dioxide nanowires with enhanced photocatalytic activity for degradation of atrazine. Appl Catal B 168–169:550–558
128. Sun B, Qiao Z, Hai Fan SK, Ai S (2013) Facile synthesis of silver sulfide/bismuth sulfide nanocomposites for photocatalytic inactivation of Escherichia coli under solar light irradiation. Mater Lett 91:142–145

129. Lydakis-Simantiris N, Riga D, Katsivela E, Mantzavinos D, Xekoukoulotakis NP (2010) Disinfection of spring water and secondary treated municipal wastewater by TiO_2 photocatalysis. Desalination 250:351–355
130. Zacarías SM, Satuf ML, Vaccari MC, Alfano OM (2015) Photocatalytic inactivation of bacterial spores using TiO_2 films with silver deposits. Chem Eng J 266:133–140
131. Wang J, Li C, Zhuang H, Zhang J (2013) Photocatalytic degradation of methylene blue and inactivation of Gramnegative bacteria by TiO_2 nanoparticles in aqueous suspension. Food Control 34:372–377
132. Vijay M, Ramachandran K, Ananthapadmanabhan PV, Nalini B, Pillai BC, Bondioli F, Manivannan A, Narendhirakannan RT (2013) Photocatalytic inactivation of Gram-positive and Gram-negative bacteria by reactive plasma processed nanocrystalline TiO_2 powder. Curr Appl Phys 13:510–516
133. Wang J, Zhuang H, Hinton A Jr, Bowker B, Zhang J (2014) Photocatalytic disinfection of spoilage bacteria Pseudomonas fluorescens and Macrococcus caseolyticus by nano-TiO_2. LWT – Food Sci Technol 59:1009–1017
134. Long M, Wang J, Zhuang H, Zhang Y, Wu H, Zhang J (2014) Performance and mechanism of standard nano- TiO_2 (P-25) in photocatalytic disinfection of foodborne microorganisms – Salmonella typhimurium and Listeria monocytogenes. Food Control 39:68–74
135. Berberidou C, Paspaltsis I, Pavlidou E, Sklaviadis T, Poulios I (2012) Heterogenous photocatalytic inactivation of B. stearothermophilus endospores in aqueous suspensions under artificial and solar irradiation. Appl Catal Environ 125:375–382
136. Schrank SG, José HJ, Moreira RFPM (2002) Simultaneous photocatalytic Cr(VI) reduction and dye oxidation in a TiO_2 slurry reactor. J Photochem Photobiol A 147:71–76
137. Umar M, Aziz HA (2013) Organic pollutants - monitoring, risk and treatment. InTech, Rijeka
138. Wang T, Wang J, Jin Y (2007) Slurry reactors for gas-to-liquid processes: a review. Ind Eng Chem Res 46:5824–5847
139. Sivaiah M, Majumder SK (2013) Hydrodynamics and mixing characteristics in an ejector-induced downflow slurry bubble column (EIDSBC). Chem Eng J 225:720–733
140. Nishio J, Tokumura M, Znad HT, Kawase Y (2006) Photocatalytic decolorization of azo-dye with zinc oxide powder in an external UV light irradiation slurry photoreactor. J Hazard Mater 138:106–115
141. McCullagh C, Robertson PKJ, Adams M, Pollard PM, Mohammed A (2010) Development of a slurry continuous flow reactor for photocatalytic treatment of industrial waste water. J Photochem Photobiol A 211:42–46
142. Subramanian M, Kannan A (2010) Photocatalytic degradation of phenol in a rotating annular reactor. Chem Eng Sci 65:2727–2740
143. Inoue T, Fujishima A, Konishi S, Honda K (1979) Photoelectrocatalytic reduction of carbon dioxide in aqueous suspensions of semiconductor powders. Nature 277:637–638
144. Tahir M, Amin NS (2013) Advances in visible light responsive titanium oxide-based photocatalysts for CO_2 conversion to hydrocarbon fuels. Energy Convers Manag 76:194–214
145. Rossetti I, Villa A, Pirola C, Prati L, Ramis G (2014) A novel high-pressure photoreactor for CO_2 photoconversion to fuels. RSC Adv 4:28883–28885
146. Priya R, Kanmani S (2009) Batch slurry photocatalytic reactors for the generation of hydrogen from sulfide and sulfite waste streams under solar irradiation. Solar Energy 83:1802–1805
147. Matthews RW (1991) Photooxidative degradation of coloured organics in water using supported catalysts. TiO_2 on sand. Water Res 25:1169–1176
148. Dhananjeyan MR, Kiwi J, Thampi KR (2000) Photocatalytic performance of TiO_2 and Fe_2O_3 immobilized on derivatized polymer films for mineralisation of pollutants. Chem Commun 15:1443–1444
149. Wang X, Shi F, Huang W, Fan C (2012) Synthesis of high quality TiO_2 membranes on alumina supports and their photocatalytic activity. Thin Solid Films 520:2488–2492

150. Sakthivel S, Shankar MV, Palanichamy M, Arabindoo B, Murugesan V (2002) Photocatalytic decomposition of leather dye: comparative study of TiO_2 supported on alumina and glass beads. J Photochem Photobiol A 148:153–159
151. Khatamian M, Hashemian S, Yavari A, Saket M (2012) Preparation of metal ion (Fe^{3+} and Ni^{2+}) doped TiO_2 nanoparticles supported on ZSM-5 zeolite and investigation of its photocatalytic activity. Mate Sci Eng 177:1623–1627
152. Li Y, Zhou X, Chen W, Li L, Zen M, Qin S, Sun S (2012) Photodecolorization of Rhodamine B on tungstendoped TiO_2/activated carbon under visible-light irradiation. J Hazard Mater 227–228:25–33
153. Zhang Y, Crittenden JC, Hand DW, Perram DL (1994) Fixed-bed photocatalysts for solar decontamination of water. Environ Sci Technol 35:435–442
154. Li D, Zhua Q, Hana C, Yanga Y, Jiangb W, Zhang Z (2015) Photocatalytic degradation of recalcitrant organic pollutants in water using a novel cylindrical multi-column photoreactor packed with TiO_2-coated silica gel beads. J Hazard Mater 285:398–408
155. Ahmed MH, Keyes TE, Byrne JA, Blackledge CW, Hamilton JW (2011) Adsorption and photocatalytic degradation of human serum albumin on TiO_2 and Ag–TiO_2 films. J Photochem Photobiol A 222:123–131
156. Pan JH, Lei Z, Lee WI, Xiong Z, Wang Q, Zhao XS (2011) Mesoporous TiO_2 photocatalytic films on stainless steel for water decontamination. Catal Sci Technol 2:147–155
157. Wang B, Karthikeyan R, Lu X-Y, Xuan J, Leung MK (2013) High photocatalytic activity of immobilized TiO_2 nanorods on carbonized cotton fibers. J Hazard Mater 263:659–669
158. Li D, Zheng H, Wang Q, Wang X, Jiang W, Zhang Z, Yang Y (2014) A novel double-cylindrical-shell photoreactor immobilized with monolayer TiO_2-coated silica gel beads for photocatalytic degradation of Rhodamine B and methyl orange in aqueous solution. Sep Purif Technol 123:130–138
159. Behnajady MA, Modirshahla N, Daneshvar N, Rabbani M (2007) Photocatalytic degradation of an azo dye in a tubular continuous-flow photoreactor with immobilized TiO_2 on glass plates. Chem Eng J 127:167–176
160. Faure M, Gerardin F, Andréa J-C, Ponsa M-N, Zahraa O (2011) Study of photocatalytic damages induced on E. coli by different photocatalytic supports (various types and TiO_2 configurations). J Photochem Photobiol A 222:323–329
161. Pablos C, Van Grieken R, Marugán J, Moreno B (2011) Photocatalytic inactivation of bacteria in a fixed-bedreactor: mechanistic insights by epifluorescence microscopy. Catal Today 161:133–139
162. Van Grieken R, Marugan J, Sordo C, Pablos C (2009) Comparison of the photocatalytic disinfection of E. coli suspensions in slurry, wall and fixed-bed reactors. Catal Today 144:48–54
163. Hsu M-H, Chang C-J (2014) S-doped ZnO nanorods on stainless-steel wire mesh as immobilized hierarchical photocatalysts for photocatalytic H_2 production. Int J Hydrog Energy 39:16524–16533
164. Augugliaro V, Loddo V, Pagliaro M, Palmisano G, Palmisano L (2010) Clean by light irradiation. RSC Publishing, Cambridge
165. Hao X-g, Li H-h, Zhang Z-l, Fan C-m, Liu S-b, Sun Y-p (2009) Modeling and experimentation of a novel labyrinth bubble photoreactor for degradation of organic pollutant. Chem Eng Res Des 87:1604–1611
166. Cernigoj U, Stangar UL, Trebse P (2007) Evaluation of a novel Carberry type photoreactor for the degradation of organic pollutants in water. J Photochem Photobiol A 188:169–176
167. Lo C-C, Huang C-W, Liao C-H, Wu JCS (2010) Novel twin reactor for separate evolution of hydrogen and oxygen in photocatalytic water splitting. Int J Hydrog Energy 35:1523–1529
168. Oralli E, Dincer I, Naterer GF (2011) Solar photocatalytic reactor performance for hydrogen production from incident ultraviolet radiation. Int J Hydrog Energy 36:9446–9452

169. Xiong Z, Zhao Y, Zhang J, Zheng C (2015) Efficient photocatalytic reduction of CO_2 into liquid products over cerium doped titania nanoparticles synthesized by a sol–gel auto-ignited method. Fuel Process Technol 135:6–13
170. Wang J, Yang C, Wang C, Han W, Zhu W (2014) Photolytic and photocatalytic degradation of micro pollutants in a tubular reactor and the reaction kinetic models. Sep Purif Technol 122:105–111
171. Reilly K, Taghipour F, Wilkinson DP (2012) Photocatalytic hydrogen production in a UV-irradiated fluidized bed reactor. Energy Procedia 29:513–521
172. Swarnalatha B, Anjaneyulu Y (2004) Studies on the heterogeneous photocatalytic oxidation of 2,6-dinitrophenol in aqueous TiO_2 suspension. J Mol Catal A 223:161–165
173. Han W, Zhang P, Zhu W, Yin J, Li L (2004) Photocatalysis of p-chlorobenzoic acid in aqueous solution under irradiation of 254 nm and 185 nm UV light. Water Res 38:4197–4203
174. Chen Y, Lu A, Li Y, Yip HY, An T, Li G, Jin P, Wonga P-K (2011) Photocatalytic inactivation of Escherichia coli by natural sphalerite suspension: effect of spectrum, wavelength and intensity of visible light. Chemosphere 84:1276–1281
175. Benabbou AK, Derriche Z, Felix C, Lejeune P, Guillard C (2007) Photocatalytic inactivation of Escherischia coli: effect of concentration of TiO_2 and microorganism, nature, and intensity of UV irradiation. Appl Catal Environ 76:257–263
176. Hernández-Gordillo A, Tzompantzi F, Oros-Ruiz S, Torres-Martinez LM, Gómez R (2014) Enhanced blue-light photocatalytic H_2 production using CdS nanofiber. Catal Commun 45:139–143
177. Gomathisankar P, Hachisuka K, Katsumata H, Suzuki T, Funasaka K, Kaneco S (2013) Enhanced photocatalytic hydrogen production from aqueous methanol solution using ZnO with simultaneous photodeposition of Cu. Int J Hydrog Energy 38:11840–11846
178. Gálvez JB, Rodríguez SM (2003) Solar detoxification. UNESCO Publishing, Paris
179. Spasiano D, Marotta R, Malato S, Fernandez-Ibanez P, Di Somma I (2015) Solar photocatalysis: materials, reactors, some commercial, and pre-industrialized applications. A comprehensive approach. Appl Catal B 170–171:90–123
180. Alfano OM, Bahnemann D, Cassano AE, Dillert R, Goslich R (2000) Photocatalysis in water environments using artificial and solar light. Catal Today 58:199–230
181. Tanveer M, Guyer GT (2013) Solar assisted photo degradation of wastewater by compound parabolic collectors: review of design and operational parameters. Renew Sustain Energy Rev 24:534–543
182. Malato S, Fernandez-Ibanez P, Maldonado MI, Blanco J, Gernjak W (2009) Decontamination and disinfection of water by solar photocatalysis: recent overview and trends. Catal Today 147:1–59
183. Keane DA, McGuigan KG, Ibáñez PF, Polo-López MI, Byrne JA, Dunlop PSM, O'Shea K, Dionysiou DD, Pillai SC (2014) Solar photocatalysis for water disinfection: materials and reactor design. Catal Sci Technol 4:1211–1226
184. Zayani G, Bousselmi L, Mhenni F, Ghrabi A (2009) Solar photocatalytic degradation of commercial textile azo dyes: performance of pilot plant scale thin film fixed-bed reactor. Desalination 246:344–352
185. Xu J, Ao Y, Fu D, Lin J, Lin Y, Shen X, Yuan C, Yin Z (2008) Photocatalytic activity on TiO_2-coated side-glowing optical fiber reactor under solar light. J Photochem Photobiol A 199:165–169
186. Vidal A, Dıaz AI, El Hraiki A, Romero M, Muguruza I, Senhaji F, González J (1999) Solar photocatalysis for detoxification and disinfection of contaminated water: pilot plant studies. Catal Today 54:283–290
187. McLoughlin OA, Kehoe SC, McGuigan KG, Duffy EF, Al Touati F, Gernjak W, Alberola IO, Rodrıguez SM, Gill LW (2004) Solar disinfection of contaminated water: a comparison of three small-scale reactors. Sol Energy 77:657–664

188. Alrousan DMA, Polo-López MI, Dunlop PSM, Fernández-Ibánez P, Byrne JA (2012) Solar photocatalytic disinfection of water with immobilised titanium dioxide in re-circulating flow CPC reactors. Appl Catal Environ 128:126–134
189. Xing Z, Zong X, Pan J, Wang L (2013) On the engineering part of solar hydrogen production from water splitting: photoreactor design. Chem Eng Sci 104:125–146
190. Jing D, Guo L, Zhao L, Zhang X, Liu H, Li M, Shen S, Liu G, Hu X, Zhang X, Zhang K, Ma L, Guo P (2010) Efficient solar hydrogen production by photocatalytic water splitting: from fundamental study to pilot demonstration. Int J Hydrog Energy 35:7087–7097
191. Villa K, Domenech X, Malato S, Maldonado MI, Peral J (2013) Heterogeneous photocatalytic hydrogen generation in a solar pilot plant. Int J Hydrog Energy 38:12718–12724
192. Malato S, Blanco J, Alarcon DC, Maldonado MI, Fernandez-Ibanez P, Gernjak W (2007) Photocatalytic decontamination and disinfection of water with solar collectors. Catal Today 122:137–149
193. Xu C, Rangaiah GP, Zhao XS (2015) A computational study of the effect of lamp arrangements on the performance of ultraviolet water disinfection reactors. Chem Eng Sci 122:299–306
194. Ray AK, Beenackers AACM (1998) Development of a new photocatalytic reactor for water purification. Catal Today 40:73–83
195. Palmisano G, Loddo V, Augugliaro V, Bellardita M, Camera Roda G, Parrino F (2015) Validation of a twodimensional modeling of an externally irradiated slurry photoreactor. Chem Eng J 262:490–498
196. Tokumura M, Znad HT, Kawase Y (2006) Modeling of an external light irradiation slurry photoreactor: UV light or sunlight-photoassisted Fenton discoloration of azo-dye Orange II with natural mineral tourmaline powder. Chem Eng Sci 61:6361–6371
197. Palmisano G, Loddo V, Augugliaro V (2013) Two-dimensional modeling of an externally irradiated slurry photoreactor. Int J Chem React Eng 11
198. Cassano AE, Martin CA, Brandi RJ, Alfano OM (1995) Photoreactor analysis and design: fundamentals and applications. Ind Eng Chem Res 34:2155–2201
199. Pozzo RL, Brandi RJ, Giombi JL, Baltanás MA, Cassano AE (2005) Design of fluidized bed photoreactors: optical properties of photocatalytic composites of titania CVD-coated onto quartz sand. Chem Eng Sci 60:2785–2794
200. Irazoqui HA, Cerdá J, Cassano AE (1976) The radiation field for the point and line source approximations and the three-dimensional source models: applications to photoreactions. Chem Eng J 11:27–37